

Design and performance analysis of channel estimators under pilot spoofing attacks in multiple-antenna systems

Donatella Darsena, *Senior Member, IEEE*, Giacinto Gelli, *Senior Member, IEEE*, Ivan Iudice, and Francesco Verde, *Senior Member, IEEE*

Abstract—In multiple antenna systems employing time-division duplexing, spatial precoder design at the base station (BS) leverages channel state information acquired through uplink pilot transmission, under the assumption of channel reciprocity. Malicious eavesdroppers can start pilot spoofing attacks to alter such design, in order to improve their eavesdropping performance in downlink. The aim of this paper is to study the effects of pilot spoofing attacks on uplink channel estimation, by assuming that the BS knows the angle of arrivals (AoAs) of the legitimate channels. Specifically, after assessing the performance of the simple least squares estimator (LSE), we consider more sophisticated estimators, such as the maximum likelihood estimator (MLE) and different versions of the minimum mean square error estimator (MMSEE), involving different degrees of *a priori* information about the pilot spoofing attacks. Theoretical analysis and numerical simulations are used to compare the performance of such estimators. In particular, we analytically demonstrate that the spoofing effects in the high signal-to-noise ratio regime can be completely suppressed, under certain conditions involving the AoAs of the legitimate and spoofing channels. Moreover, we show that even an imperfect knowledge of the AoAs and of the average transmission power of the spoofing signals allows the MLE and MMSEE to achieve significant performance gains over the LSE.

Index Terms—Array processing, channel estimation, least squares, maximum likelihood, minimum mean square error, multiple antenna systems, physical-layer security, pilot spoofing.

I. INTRODUCTION

MULTIPLE transmit/receive antennas is a well-established technology to design high-speed reliable wireless communication links [1]. In terms of spectral efficiency, a multiple-antenna system can approach the Shannon capacity of the wireless channel, provided that channel state information (CSI) is available at both ends of the communication link [2], [3]. In particular, design of

effective transmit beamformers for the downlink channel requires knowledge of the CSI at the base station (BS). A widely-adopted approach for acquiring CSI at the BS in time-division duplexing (TDD) systems relies on channel reciprocity. Standard TDD beamforming protocols involve two phases: in the *training phase*, the users transmit known (*pilot* or *training*) symbols to the BS in the uplink; in the *data phase*, the BS estimates the uplink channels and, capitalizing on channel reciprocity, forms the downlink data beams to the users, by using the estimated uplink channels. TDD beamforming is expected to play a significant role in forthcoming 5G systems [4], especially when working at millimeter-wave frequencies and with a huge number of antenna elements at the BS (*massive MIMO* systems).

Uplink training sessions in TDD systems are vulnerable to malicious attacks aimed at altering their operation [5]. Specifically, *intelligent* eavesdroppers can significantly enhance their wiretapping capability in downlink by mounting *pilot spoofing attacks* in uplink [6]. With reference to Fig. 1, we consider a scenario encompassing a multi-antenna BS, referred to as *Alice*, multiple legitimate single-antenna users, referred to as *Bobs*, and multiple single-antenna eavesdroppers, referred to as *Eves*. The eavesdroppers in Fig. 1 are intelligent in the sense that they can act both as passive nodes (i.e., they try to intercept confidential communications in downlink) as well as active ones (i.e., they can transmit pilot signals in uplink). Specifically, the aim of each Eve is to steal information from a particular Alice-to-Bob downlink transmission during the data phase, thus acting as a passive terminal. With this goal in mind, each Eve mounts a spoofing attack during the training phase, by transmitting the same pilot sequence as the selected Bob, thus operating as an active node. In this paper, we focus on such pilot attacks during the uplink training phase and study the performance of the channel estimation process at Alice, by assuming that Bobs employ orthogonal pilot sequences.

Several papers have dealt with the problem of combating pilot spoofing attacks [7]–[15], [17], [18]. In all such papers, a common belief is that, if Eves attack the uplink training phase by transmitting the same training sequence as Bobs, the channel estimation process at Alice is irreparably compromised. Henceforth, all the efforts in [7]–[15], [17], [18] have been mainly directed towards detection of the Eves' attacks and relative countermeasures. In particular, an energy-ratio-based detector has been proposed in [9] to detect a spoofing attack,

Manuscript received December 26, 2019; revised March 28, 2020; accepted March 30, 2020. Date of publication XX YY, 2020; date of current version March 31, 2020. The associate editor coordinating the review of this manuscript and approving it for publication was Prof. Tobias Oechtering. (Corresponding author: Francesco Verde).

D. Darsena is with the Department of Engineering, Parthenope University, Naples I-80143, Italy (e-mail: darsena@uniparthenope.it). G. Gelli and F. Verde are with the Department of Electrical Engineering and Information Technology, University Federico II, Naples I-80125, Italy [e-mail: (gelli,f.verde)@unina.it]. I. Iudice is with Italian Aerospace Research Centre (CIRA), Capua I-81043, Italy (e-mail: i.iudice@cira.it).

D. Darsena, G. Gelli, and F. Verde are also with National Inter-University Consortium for Telecommunications (CNIT).

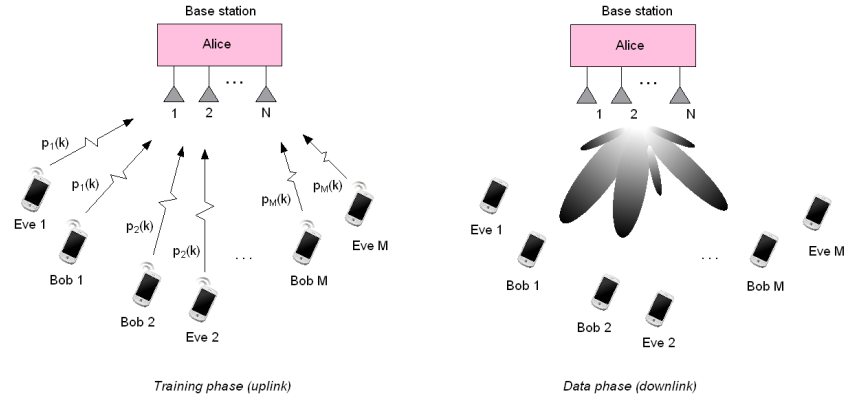


Fig. 1. Single-antenna eavesdroppers (Eves) launch pilot spoofing attacks during the uplink training phase between legitimate single-antenna users (Bobs) and a multi-antenna BS (Alice), with the aim of modifying beam design in order to intercept information in the subsequent downlink data phase.

which explores the asymmetry of the received signal power levels between Bob and Alice. An attack can be additionally detected by resorting to the source enumeration approach [11] and the minimum description length criterion [14]. To mitigate the effects of spoofing, estimation of both Bob and Eve channels has been studied in [15], along with secure beamforming. A random channel training scheme has been proposed in [16], where multiple orthogonal pilot sequences are simultaneously allocated to Bob, who randomly selects one pilot sequence to transmit. A remarkable extension of [15] and [16] to a multiuser scenario has been developed in [18].

Although all the aforementioned works have collectively provided a significant research progress on counteracting pilot spoofing attacks, they did not study in detail the effects of spoofing on channel estimation performance. Moreover, in such papers, the adopted fading channel models do not incorporate detailed spatial information, such as the angle-of-arrivals (AoAs), which will be shown in the following to play a central role when assessing the legitimate channel estimation performance under a spoofing attack.

In this paper, we resort to angle-dependent multipath fading channel models for the Bobs-to-Alice and Eves-to-Alice links, by assuming that the AoAs of the legitimate Bobs-to-Alice channels are known at Alice. Moreover, we consider *least squares (LS)*, *maximum likelihood (ML)*, and *minimum mean square error (MMSE)* channel estimators [19].

LS and ML estimators belong to the family of the classical estimation approaches, for which the legitimate channels are viewed as *deterministic but unknown* vectors. In the case of the LS estimator (LSE), which is the easiest type of estimator to analyze and understand, the existence of the spoofing signals is ignored and, thus, no information about the pilot spoofing attacks is required at Alice. On the other hand, when the spoofing signals are treated as purely noise for the derivation of the ML estimator (MLE), knowledge of the correlation matrix of each spoofing-plus-noise contribution is also required.

Following the *Bayesian approach*, three MMSE estimators (MMSEs) are further studied in this paper by regarding the legitimate channels as *random* vectors whose particular realizations have to be estimated. For each Bob-to-Alice channel, the (optimal) MMSE estimator (MMSEE) minimizes the

Bayesian mean squared error (BMSE), where the average is taken not only over the data – which also includes the contribution of the corresponding Eve – but over the probability density function (pdf) of the legitimate channel vector as well, without imposing any constraint on the structure of the estimator. The MMSEE has prior information on the legitimate channels and exploits this information to outperform the MLE, especially for low-to-moderate signal-to-noise ratio (SNR) values.

The remaining two MMSEs are developed when Alice is supposed to be aware of the pilot spoofing attacks: namely, Alice has *a priori* estimates of the AoAs and average transmission power of each spoofing signal, and she knows the statistical characterization of the corresponding estimation errors. In this case, for each Bob-to-Alice channel, the estimator minimizing the Bayesian MSE – where the average is now taken over the joint pdf of the legitimate channel, the data, and the estimation errors of the corresponding Eve’s parameters – does not admit a closed-form expression. To obtain mathematically tractable solutions, we retain the Bayesian MMSE criterion but constrain the estimators to be linear.

With reference to a given Bob-Eve pair, the contribution of this paper is threefold:

- 1) We show analytically that the LSE does not have spoofing suppression capabilities, even in the absence of noise, whereas the MLE can perfectly reject the spoofing pilots of Eve in the high-SNR region, provided that the subspaces generated by the columns of the steering matrices of the legitimate and spoofing channels are nonoverlapping.
- 2) We analytically demonstrate that, if the AoAs through the multipath Bob-to-Alice and Eve-to-Alice channels are all distinct, the MMSEE is able to cancel the spoofing signal in the high-SNR regime. The synthesis of the MLE and MMSEE involves the knowledge of the correlation matrix of the received data. We discuss how in principle such a matrix can be estimated and, hence, MLE and MMSEE can be implemented without requiring awareness of the pilot spoofing attack.
- 3) We develop two (suboptimal) linear MMSEs (LMMSEs) estimators: the former one, which is referred to as *naive* LMMSEE, is synthesized by relying on estimates of the AoAs and average transmission power of Eve, without

making use of the statistical characterization of the corresponding estimation errors; the latter one, which is referred to as *improved* LMMSE, besides using the estimates of the Eve's parameters, also exploits the knowledge of the pdf of the estimation errors. We prove that the naive LMMSEE exhibits a serious performance degradation in the high SNR regime, whereas its improved version is fairly resistant to the pilot spoofing attack.

The paper is organized as follows. The next section describes the signal model and introduces some basic assumptions. Section III revisits LSE and MLE, and reports a theoretical analysis of their spoofing suppression capabilities. The performance of the MMSEE and its implementation from data are studied in Section IV; naive and improved LMMSEs are developed in the same section starting from estimates of the Eve's parameters. Section V discusses analytical and simulation results in terms of BMSE and secrecy rate, and Section VI offers some conclusions.

A. Notations

Upper- and lower-case bold letters denote matrices and vectors; the superscripts $*$, T , H , -1 , and \dagger denote the conjugate, the transpose, the Hermitian (conjugate transpose), the inverse, and the Moore-Penrose generalized inverse [20] of a matrix; \mathbb{C} , \mathbb{R} and \mathbb{Z} are the fields of complex, real and integer numbers; \mathbb{C}^n [\mathbb{R}^n] denotes the vector-space of all n -column vectors with complex [real] coordinates; similarly, $\mathbb{C}^{n \times m}$ [$\mathbb{R}^{n \times m}$] denotes the vector-space of all the $n \times m$ matrices with complex [real] elements; $\text{erf}(\cdot)$ denotes the error function [21]; $\delta(n)$ is the Kronecker delta, i.e., $\delta(n) = 1$ when $n = 0$ and zero otherwise; $\log_a(\cdot)$ is taken to the base a [we also use the shorthand $\ln(\cdot)$ for $\log_e(\cdot)$] and $j \triangleq \sqrt{-1}$ denotes the imaginary unit; $\mathbf{0}_n$, $\mathbf{O}_{n \times m}$ and \mathbf{I}_n denote the n -column zero vector, the $n \times m$ zero matrix and the $n \times n$ identity matrix; \otimes denotes the Kronecker product between two matrices [22]; for any $\mathbf{A} \in \mathbb{C}^{n \times m}$, $\text{rank}(\mathbf{A})$ and $\text{trace}(\mathbf{A})$ denote the rank and the trace of \mathbf{A} ; for any $\mathbf{A} \in \mathbb{C}^{n \times m}$, $\|\mathbf{A}\| \triangleq [\text{trace}(\mathbf{A} \mathbf{A}^H)]^{1/2}$ denotes the (induced) Frobenius norm of \mathbf{A} [23]; matrix $\mathbf{A} = \text{diag}(a_0, a_1, \dots, a_{p-1}) \in \mathbb{C}^{p \times p}$ is diagonal; $\frac{\partial}{\partial \mathbf{A}^*} f \in \mathbb{C}^{n \times m}$ is the *gradient* of the real-valued scalar function f with respect to $\mathbf{A}^* \in \mathbb{C}^{n \times m}$ [24]; the operator $\text{vec}(\mathbf{A}) \triangleq [\mathbf{a}_1^T, \mathbf{a}_2^T, \dots, \mathbf{a}_m^T]^T \in \mathbb{C}^{nm}$ creates a column vector from the matrix $\mathbf{A} = [\mathbf{a}_1, \mathbf{a}_2, \dots, \mathbf{a}_m] \in \mathbb{C}^{n \times m}$ by stacking the column vectors of \mathbf{A} ; $\mathcal{N}(\mathbf{A})$, $\mathcal{R}(\mathbf{A})$, and $\mathcal{R}^\perp(\mathbf{A})$ denote the null space, the range (column space), and the orthogonal complement of the column space of $\mathbf{A} \in \mathbb{C}^{n \times m}$ in \mathbb{C}^n ; $\mathbb{E}[\cdot]$ denotes ensemble averaging and, finally, a circularly symmetric complex Gaussian random vector $\mathbf{x} \in \mathbb{C}^n$ with mean $\boldsymbol{\mu} \in \mathbb{C}^n$ and covariance matrix $\mathbf{R} \in \mathbb{C}^{n \times n}$ is denoted as $\mathbf{x} \sim \mathcal{CN}(\boldsymbol{\mu}, \mathbf{R})$.

II. SYSTEM MODEL AND PRELIMINARIES

As shown in Fig. 1, our scenario encompasses one BS (Alice) equipped with N receive antennas, M legitimate single-antenna users (Bobs) and M single-antenna eavesdroppers (Eves). Bobs use orthogonal pilot sequences for channel estimation: specifically, for $\mathcal{K} \triangleq \{0, 1, \dots, K-1\}$

and $\mathcal{M} \triangleq \{1, 2, \dots, M\}$, let $p_m(k) \in \mathbb{C}$ denote the pilot symbol transmitted by the m th Bob within the k th symbol interval, with average transmission power (per symbol) $\mathcal{P}_{B,m}$ and $K \geq 1$ [25].¹ Orthogonality among the pilot sequences means that $\mathbf{p}_{m_1}^H \mathbf{p}_{m_2} = \delta(m_1 - m_2)$ where $\mathbf{p}_m \triangleq [p_m(0), p_m(1), \dots, p_m(K-1)]^T \in \mathbb{C}^K$ is the pilot vector of the m th Bob. The vector \mathbf{p}_m is known to the m th Eve, which concurrently sends the same pilot block in the training phase with average transmission power $\mathcal{P}_{E,m}$. Moreover, $\mathbf{p}_1, \mathbf{p}_2, \dots, \mathbf{p}_M$ are perfectly known at Alice.

We assume that no appreciable local scattering occurs at Alice and, hence, fading at its antennas is spatially correlated. Such an assumption is reasonable [26] when the BS is sufficiently high above the ground. In this case, for narrowband signals, the angle-dependent multipath fading single-input multiple-output (SIMO) baseband channel between the generic transmitter $\text{TX} \in \{\text{B}, \text{E}\}$ and Alice can be modeled as

$$\tilde{\mathbf{h}}_{\text{TX},m} = \frac{1}{\sqrt{L_{\text{TX},m}}} \sum_{\ell=1}^{L_{\text{TX},m}} \mathbf{a}(\theta_{\text{TX},\ell,m}) h_{\text{TX},\ell,m} \quad (1)$$

where $L_{\text{TX},m} \in \mathbb{N}$ is the number of paths between the m th transmitter and Alice, $\mathbf{a}(\theta_{\text{TX},\ell,m}) \in \mathbb{C}^N$ and $h_{\text{TX},\ell,m} \in \mathbb{C}$ denote the steering vector and the gain of the ℓ th path of the m th Bob, respectively, with $\theta_{\text{TX},\ell,m}$ being the corresponding AoA. For the sake of simplicity, we assume a uniform linear array (ULA) at Alice.² The (normalized) steering vector $\mathbf{a}(\theta_{\text{TX},\ell,m})$ can be expressed [27] as shown at the top of the next page in (2), with

$$\Psi_n(\theta_{\text{TX},\ell,m}) \triangleq -n \frac{d}{\lambda_c} \cos(\theta_{\text{TX},\ell,m}) \quad (3)$$

for $n \in \{0, 1, \dots, N-1\}$, where d is the absolute antenna spacing and λ_c is the signal wavelength. We assume that legitimate and spoofing signals are perfectly synchronized [5].

The discrete-time signal vector $\mathbf{y}(k) \in \mathbb{C}^N$ received by Alice within the k th symbol period can be expressed as

$$\mathbf{y}(k) = \sum_{m=1}^M \left(\sqrt{\mathcal{P}_{B,m}} \mathbf{A}_{B,m} \mathbf{h}_{B,m} + \sqrt{\mathcal{P}_{E,m}} \mathbf{A}_{E,m} \mathbf{h}_{E,m} \right) p_m(k) + \mathbf{v}(k) \quad (4)$$

with $k \in \mathcal{K}$, where, for $\text{TX} \in \{\text{B}, \text{E}\}$,

$$\mathbf{A}_{\text{TX},m} \triangleq \frac{1}{\sqrt{L_{\text{TX},m}}} [\mathbf{a}(\theta_{\text{TX},1,m}), \mathbf{a}(\theta_{\text{TX},2,m}), \dots, \mathbf{a}(\theta_{\text{TX},L_{\text{TX},m},m})] \in \mathbb{C}^{N \times L_{\text{TX},m}} \quad (5)$$

$$\mathbf{h}_{\text{TX},m} \triangleq [h_{\text{TX},1,m}, h_{\text{TX},2,m}, \dots, h_{\text{TX},L_{\text{TX},m},m}]^T \in \mathbb{C}^{L_{\text{TX},m}} \quad (6)$$

and $\mathbf{v}(k) \sim \mathcal{CN}(\mathbf{0}_N, \sigma_v^2 \mathbf{I}_N)$ is additive white Gaussian noise, with $\mathbf{v}(k_1)$ and $\mathbf{v}(k_2)$ statistically independent of each other for $k_1 \neq k_2 \in \mathcal{K}$. Hereinafter, $\mathbf{A}_{\text{TX},m}$ is referred to as the m th *steering matrix*. We assume a Rayleigh fading model, according to which $\mathbf{h}_{B,m} \sim \mathcal{CN}(\mathbf{0}_{L_{B,m}}, \mathbf{I}_{L_{B,m}})$ and

¹Throughout the paper, we use the convention that the subscripts B and E indicate a quantity referring to Bobs and Eves, respectively.

²Our framework can be extended to nonuniform arrays as well.

$$\mathbf{a}(\theta_{\text{TX},\ell,m}) = \frac{[e^{j2\pi\Psi_0(\theta_{\text{TX},\ell,m})}, e^{j2\pi\Psi_1(\theta_{\text{TX},\ell,m})}, \dots, e^{j2\pi\Psi_{N-1}(\theta_{\text{TX},\ell,m})}]^T}{\sqrt{N}} \quad (2)$$

$\mathbf{h}_{E,m} \sim \mathcal{CN}(\mathbf{0}_{L_{E,m}}, \mathbf{I}_{L_{E,m}})$ are mutually independent vectors, statistically independent of $\mathbf{v}(k)$, $\forall k \in \mathcal{K}$ and $\forall m \in \mathcal{M}$.

Let us gather all the data (4) received during the uplink pilot phase in $\mathbf{Y} \triangleq [\mathbf{y}(0), \mathbf{y}(1), \dots, \mathbf{y}(K-1)] \in \mathbb{C}^{N \times K}$, thus obtaining the signal model³

$$\mathbf{Y} = \sum_{m=1}^M \left(\sqrt{\mathcal{P}_{B,m}} \mathbf{A}_{B,m} \mathbf{h}_{B,m} + \sqrt{\mathcal{P}_{E,m}} \mathbf{A}_{E,m} \mathbf{h}_{E,m} \right) \mathbf{p}_m^T + \mathbf{V} \quad (7)$$

where $\mathbf{V} \triangleq [\mathbf{v}(0), \mathbf{v}(1), \dots, \mathbf{v}(K-1)] \in \mathbb{C}^{N \times K}$.

Let us focus on the channel estimation process of the \bar{m} th user, with $\bar{m} \in \mathcal{M}$. In this case, by capitalizing on the orthogonality among the pilot vectors, Alice performs the correlation of the received data \mathbf{Y} with $\mathbf{p}_{\bar{m}}$, thus obtaining

$$\mathbf{y}_{\bar{m}} \triangleq \mathbf{Y} \mathbf{p}_{\bar{m}}^* = \mathbf{K}_{B,\bar{m}} \mathbf{h}_{B,\bar{m}} + \mathbf{K}_{E,\bar{m}} \mathbf{h}_{E,\bar{m}} + \mathbf{v}_{\bar{m}} \quad (8)$$

where we have defined $\mathbf{K}_{B,\bar{m}} \triangleq \sqrt{\mathcal{P}_{B,\bar{m}}} \mathbf{A}_{B,\bar{m}} \in \mathbb{C}^{N \times L_{B,\bar{m}}}$ and $\mathbf{K}_{E,\bar{m}} \triangleq \sqrt{\mathcal{P}_{E,\bar{m}}} \mathbf{A}_{E,\bar{m}} \in \mathbb{C}^{N \times L_{E,\bar{m}}}$, and, by assumption, $\mathbf{v}_{\bar{m}} \triangleq \mathbf{V} \mathbf{p}_{\bar{m}}^* \sim \mathcal{CN}(\mathbf{0}_N, \sigma_v^2 \mathbf{I}_N)$.

To simplify the notation, in the remaining part of the paper, we will drop the subscript \bar{m} in (1)–(3), (5)–(6), and (8), and study different estimation strategies for reliably acquiring the CSI of a generic Bob-to-Alice uplink in order to design a suitable beamformer for the subsequent Alice-to-Bobs downlink data transmission. In all the considered cases, we assume that Alice has perfect knowledge of the composite matrix \mathbf{K}_B (depending on the transmit power \mathcal{P}_B and the steering matrix \mathbf{A}_B). While \mathcal{P}_B is a system parameter that is known *a priori*, the matrix \mathbf{A}_B has to be estimated by Alice. However, such a steering matrix varies much slower than \mathbf{h}_B and, thus, it can be estimated [28]–[30] in practice during a secure setup session. Consequently, the matter boils down to estimate \mathbf{h}_B .⁴

In this paper, we study two different estimation strategies: in the former one, following the classical approach, the entries of \mathbf{h}_B are assumed to be deterministic but unknown constants; in the latter one, according to the Bayesian philosophy, the knowledge of the pdf of \mathbf{h}_B is exploited to estimate its particular realization. As a performance measure of the considered estimators, we resort to the BMSE, which is defined as

$$\text{BMSE}(\hat{\mathbf{h}}_B) \triangleq \mathbb{E} \left[\left\| \hat{\mathbf{h}}_B - \mathbf{h}_B \right\|^2 \right] \quad (9)$$

where $\hat{\mathbf{h}}_B \in \mathbb{C}^{L_B}$ denotes an estimate of \mathbf{h}_B and, unless otherwise specified, the expectation is taken with respect to

³For $\text{TX} \in \{\text{B}, \text{E}\}$, $\mathcal{P}_{\text{TX},m}$ also represents the average received power during the training phase, since $\mathbb{E}[\|\mathbf{A}_{\text{TX},m} \mathbf{h}_{\text{TX},m} \mathbf{p}^T\|^2] = 1$.

⁴In principle, Alice may perform a channel-unaware beamforming in downlink by relying only on the knowledge of \mathbf{K}_B , so-called *angular beamforming*, at the price of a capacity degradation [31]. Such a degradation might be even more severe in terms of secrecy capacity in the presence of malicious Eves.

the pdf of the triple $(\mathbf{h}_B, \mathbf{h}_E, \mathbf{v})$.⁵

III. LEAST SQUARES AND MAXIMUM LIKELIHOOD ESTIMATORS

The channel estimators derived herein are based on the assumption that both \mathbf{h}_B and \mathbf{K}_E are deterministic but unknown quantities. In this case, we can develop different *unbiased* estimators on the basis of the amount of knowledge regarding the spoofing attack. When Alice is unaware of the Eve's presence, the LSE can be used by Alice to estimate \mathbf{h}_B . On the other hand, if Alice has perfect knowledge of the correlation matrix of the *disturbance* (i.e., *spoofing signal plus noise*) (see the forthcoming discussion), it can implement the MLE to accomplish the same task.

A. Least squares estimator

The LSE is defined [19] as

$$\hat{\mathbf{h}}_{B,\text{LS}} \triangleq \arg \min_{\mathbf{h}_B \in \mathbb{C}^{L_B}} \|\mathbf{y} - \mathbf{K}_B \mathbf{h}_B\|^2. \quad (10)$$

Under the assumption that \mathbf{K}_B is full-column rank, i.e., $\text{rank}(\mathbf{K}_B) = \text{rank}(\mathbf{A}_B) = L_B$, the LSE is *unique* and it can be written as (see [19])

$$\hat{\mathbf{h}}_{B,\text{LS}} = (\mathbf{K}_B^H \mathbf{K}_B)^{-1} \mathbf{K}_B^H \mathbf{y}. \quad (11)$$

Since \mathbf{A}_B is a Vandermonde-like matrix, the condition $\text{rank}(\mathbf{K}_B) = \text{rank}(\mathbf{A}_B) = L_B$ is fulfilled [23] if $N \geq L_B$ and $\theta_{B,1} \neq \theta_{B,2} \neq \dots \neq \theta_{B,L_B}$ (i.e., the AoAs through the multipath channel between Bob and Alice are distinct). On the other hand, if $\text{rank}(\mathbf{K}_B) < L_B$, problem (10) has infinitely many solutions and \mathbf{h}_B is not identifiable, i.e., if $\hat{\mathbf{h}}_{B,\text{LS}}$ is a solution of (10) and $\alpha \in \mathcal{N}(\mathbf{K}_B)$, then $\hat{\mathbf{h}}_{B,\text{LS}} + \alpha$ is another solution of (10). The synthesis of the LSE involves knowledge of \mathbf{K}_B only and its computational burden is dominated by the matrix inversion in (11), which involves $\mathcal{O}(L_B^3)$ floating point operations (flops) [32] if computed from scratch.

The LSE (11) is unbiased and, by using the properties of the Kronecker product and the trace operator, its BMSE (9) can be expressed as follows

$$\text{BMSE}_{\text{LS}} \triangleq \frac{\text{trace} \left[\mathbf{A}_B (\mathbf{A}_B^H \mathbf{A}_B)^{-2} \mathbf{A}_B^H \mathbf{A}_E \mathbf{A}_E^H \right]}{\text{SSR}} + \frac{\text{trace} \left[(\mathbf{A}_B^H \mathbf{A}_B)^{-1} \right]}{\text{SNR}_B} \quad (12)$$

where we have defined the SNR of the Bob transmission as $\text{SNR}_B \triangleq \mathcal{P}_B / \sigma_v^2$, whereas $\text{SSR} \triangleq \mathcal{P}_B / \mathcal{P}_E$ represents the signal-to-spoofing ratio (SSR). It is noteworthy from (12) that, in the

⁵The BMSE is a reasonable performance metric in fading channels not only for Bayesian estimators, but also for the classical ones that are designed under the deterministic assumption for \mathbf{h}_B .

absence of noise, i.e., as σ_v^2 approaches to zero, the BMSE of the LSE exhibits a saturation effect, namely, a floor given by

$$\begin{aligned} \overline{\text{BMSE}}_{\text{LS}} &\triangleq \lim_{\sigma_v^2 \rightarrow 0} \text{BMSE}_{\text{LS}} \\ &= \frac{\text{trace} \left[\mathbf{A}_B (\mathbf{A}_B^H \mathbf{A}_B)^{-2} \mathbf{A}_B^H \mathbf{A}_E \mathbf{A}_E^H \right]}{\text{SSR}} \end{aligned} \quad (13)$$

which is due to the malicious pilot transmission of Eve. The following lemma provides bounds on $\overline{\text{BMSE}}_{\text{LS}}$.

Lemma 3.1: The BMSE floor of (11) is bounded as

$$\frac{1}{\text{SSR}} \sum_{\ell=1}^{L_B} \frac{\sigma_{N-\ell+1}^2(\mathbf{A}_E)}{\sigma_\ell^2(\mathbf{A}_B)} \leq \overline{\text{BMSE}}_{\text{LS}} \leq \frac{1}{\text{SSR}} \sum_{\ell=1}^{L_B} \frac{\sigma_\ell^2(\mathbf{A}_E)}{\sigma_\ell^2(\mathbf{A}_B)} \quad (14)$$

where $\sigma_1(\mathbf{A}_B) \leq \sigma_2(\mathbf{A}_B) \leq \dots \leq \sigma_{L_B}(\mathbf{A}_B)$ are the *nonzero* singular values of \mathbf{A}_B arranged in increasing order and $\sigma_1(\mathbf{A}_E) \geq \sigma_2(\mathbf{A}_E) \geq \dots \geq \sigma_N(\mathbf{A}_E)$ are the singular values of \mathbf{A}_E arranged in decreasing order.

Proof: See Appendix A. ■

Lemma 3.1 enlightens that the spoofing attack might seriously affect the performance of (11), which depends not only on the SSR, but also on the ratio between the singular values of \mathbf{A}_E and \mathbf{A}_B . In particular, the lower bound in (14) shows that, except for the limit case $\text{SSR} \rightarrow +\infty$, the floor $\overline{\text{BMSE}}_{\text{LS}}$ cannot be zero if the L_B smallest singular values of \mathbf{A}_E are nonzero. This happens when the rank of \mathbf{A}_E is greater than the number of paths between Bob and Alice, that is, compared to the legitimate channel, the spoofing one is characterized by a richer scattering with significant multipath components.

B. Maximum likelihood estimator

Let $p(\mathbf{y}; \mathbf{h}_B)$ denote the pdf of \mathbf{y} , parameterized by \mathbf{h}_B . The MLE is the solution of the maximization problem

$$\hat{\mathbf{h}}_{B,\text{ML}} \triangleq \arg \max_{\mathbf{h}_B \in \mathbb{C}^{L_B}} p(\mathbf{y}; \mathbf{h}_B). \quad (15)$$

Since the disturbance $\mathbf{d} \triangleq \mathbf{K}_E \mathbf{h}_E + \mathbf{v} \sim \mathcal{CN}(\mathbf{0}_N, \mathbf{R}_{\text{dd}})$, with $\mathbf{R}_{\text{dd}} \triangleq \mathbb{E}[\mathbf{d} \mathbf{d}^H] = \mathbf{K}_E \mathbf{K}_E^H + \sigma_v^2 \mathbf{I}_N$ being its correlation matrix (depending on \mathbf{K}_E), it results that $\hat{\mathbf{h}}_{B,\text{ML}}$ is the solution of the matrix equation (see, e.g., [19])

$$(\mathbf{K}_B^H \mathbf{R}_{\text{dd}}^{-1} \mathbf{K}_B) \hat{\mathbf{h}}_{B,\text{ML}} = \mathbf{K}_B^H \mathbf{R}_{\text{dd}}^{-1} \mathbf{y}. \quad (16)$$

If \mathbf{K}_B is full-column rank, the MLE is unique and given by

$$\hat{\mathbf{h}}_{B,\text{ML}} = (\mathbf{K}_B^H \mathbf{R}_{\text{dd}}^{-1} \mathbf{K}_B)^{-1} \mathbf{K}_B^H \mathbf{R}_{\text{dd}}^{-1} \mathbf{y}. \quad (17)$$

On the other hand, if the columns of \mathbf{K}_B are linearly dependent, there exists an infinite number of solutions for (16) that generate the same density function and, thus, similarly to the LSE, \mathbf{h}_B is not identifiable in this case.

Compared to the LSE in (11), the MLE requires the additional knowledge of the correlation matrix of the disturbance, which in its turn depends on the noise variance σ_v^2 and the composite matrix \mathbf{K}_E (determined by the transmit power \mathcal{P}_E and the steering matrix \mathbf{A}_E). The noise variance σ_v^2 is related to the noise figure of Alice and, thus, it can be known *a priori* or estimated previously. On the other hand, both \mathcal{P}_E and \mathbf{A}_E are unknown at Alice. In principle, one can estimate \mathbf{R}_{dd} from

the received data, by observing that the correlation matrix of \mathbf{y} can be expressed as

$$\mathbf{R}_{\mathbf{y}\mathbf{y}} \triangleq \mathbb{E}[\mathbf{y} \mathbf{y}^H] = \mathbf{K}_B \mathbf{K}_B^H + \mathbf{R}_{\text{dd}}. \quad (18)$$

Given a *sample* estimate $\mathbf{S}_{\mathbf{y}\mathbf{y}}$ of $\mathbf{R}_{\mathbf{y}\mathbf{y}}$ and knowledge of \mathbf{K}_B , a corresponding sample estimate of \mathbf{R}_{dd} can be obtained as $\mathbf{S}_{\text{dd}} = \mathbf{S}_{\mathbf{y}\mathbf{y}} - \mathbf{K}_B \mathbf{K}_B^H$. Estimation of $\mathbf{R}_{\mathbf{y}\mathbf{y}}$ from the received data will be discussed in Subsection IV-A. Since N is typically much larger than L_B , the computational complexity of the MLE is mainly dictated by the inversion of \mathbf{R}_{dd} , which requires $\mathcal{O}(N^3)$ flops if one resorts to batch algorithms.

The MLE (17) is unbiased and its BMSE (9) can be expressed [19] as

$$\text{BMSE}_{\text{ML}} = \text{trace} \left[(\mathbf{K}_B^H \mathbf{R}_{\text{dd}}^{-1} \mathbf{K}_B)^{-1} \right]. \quad (19)$$

The MLE is also an efficient estimator since it attains the *standard* (i.e., for *nonrandom parameter estimation*) Cramer-Rao lower bound (CRLB) [19], that is $\text{BMSE}_{\text{ML}} \leq \text{BMSE}(\hat{\mathbf{h}}_B)$, for any unbiased estimator $\hat{\mathbf{h}}_B$ of \mathbf{h}_B . In particular, in the considered scenario, one gets $\text{BMSE}_{\text{ML}} \leq \text{BMSE}_{\text{LS}}$.

Similarly to the LSE, our aim is to characterize the spoofing suppression capabilities of the MLE in the high-SNR regime. Such a characterization is provided by the following lemma.

Lemma 3.2: If the subspaces $\mathcal{R}(\mathbf{A}_B)$ and $\mathcal{R}(\mathbf{A}_E)$ are *nonoverlapping* or *disjoint*, i.e.,

$$\mathcal{R}(\mathbf{A}_B) \cap \mathcal{R}(\mathbf{A}_E) = \{\mathbf{0}_N\} \quad (20)$$

then perfect spoofing cancellation is achieved in the absence of noise, that is

$$\overline{\text{BMSE}}_{\text{ML}} \triangleq \lim_{\sigma_v^2 \rightarrow 0} \text{BMSE}_{\text{ML}} = 0. \quad (21)$$

Proof: See Appendix B. ■

A consequence of the above lemma is that, for (20) to hold, it suffices that the columns of \mathbf{A}_B and \mathbf{A}_E are linearly independent so that the (augmented) matrix $[\mathbf{A}_B, \mathbf{A}_E] \in \mathbb{C}^{N \times (L_B + L_E)}$ has full column rank. This condition is fulfilled if $N \geq L_B + L_E$ and $\theta_{B,1} \neq \dots \neq \theta_{B,L_B} \neq \theta_{E,1} \neq \dots \neq \theta_{E,L_E}$, i.e., the AoAs of the multipath Bob-to-Alice and Eve-to-Alice channels are all distinct. In a nutshell, we can state that, compared to the LSE, the MLE can effectively counteract the pilot spoofing attack, at the price however of requiring the knowledge of the correlation matrix of the spoofing-plus-noise signal.

When condition (20) is not satisfied, i.e., the AoA ranges of Bob and Eve are overlapping, perfect spoofing cancellation is impossible, even in the absence of noise. However, overlapping between the subspaces $\mathcal{R}(\mathbf{A}_B)$ and $\mathcal{R}(\mathbf{A}_E)$ depends on the distribution of the AoAs, which is governed by the physical propagation environment, as well as on the locations of Bob and Eve. Therefore, it is unlikely that condition (20) is violated at all times, due to the random transmitter locations and scattering effects. Moreover, numerical results in Section V show that the MLE is robust when the difference between the angles of incidence at which Bob and Eve arrive at Alice tends to zero for a given path.

IV. MINIMUM MEAN SQUARE ERROR ESTIMATORS

In this section, we consider the Bayesian approach to statistical estimation [19], by capitalizing on the fact that $\mathbf{h}_B \sim \mathcal{CN}(\mathbf{0}_{L_B}, \mathbf{I}_{L_B})$. Such an approach is different from the classical one pursued in Section III. Compared to LSE and MLE, Bayesian estimators improve estimation accuracy by exploiting *a priori* information about the pdf of \mathbf{h}_B . Moreover, the class of Bayesian estimators is not restricted to the unbiased ones [33], [34].

Herein, we consider three different MMSEs based on different *a priori* information about the attack of Eve. In the first one, Alice does not have any information regarding \mathbf{K}_E , which is modeled as a deterministic but unknown matrix (as already done in Section III). In the second one, it is assumed that Alice has an imperfect knowledge $\hat{\mathbf{K}}_E$ of \mathbf{K}_E . In the third one, besides $\hat{\mathbf{K}}_E$, Alice also knows the statistical characterization of the corresponding error.

A. Case 1: No *a priori* knowledge about \mathbf{K}_E

Under the assumption that \mathbf{K}_E is deterministic, the optimal MMSEE minimizes (9) and is given [19] by the mean of the posterior distribution of \mathbf{h}_B , i.e.,

$$\hat{\mathbf{h}}_{B, \text{MMSE}} = \mathbb{E}[\mathbf{h}_B | \mathbf{y}]. \quad (22)$$

In this case, the vectors \mathbf{y} and \mathbf{h}_B are jointly complex Gaussian and, hence, the conditional distribution of $\mathbf{h}_B | \mathbf{y}$ is complex Gaussian, too. Therefore, the MMSEE (22) turns out to be *linear* and assumes the form (see, e.g., [19])

$$\begin{aligned} \hat{\mathbf{h}}_{B, \text{MMSE}} &= (\mathbf{I}_{L_B} + \mathbf{K}_B^H \mathbf{R}_{\text{dd}}^{-1} \mathbf{K}_B)^{-1} \mathbf{K}_B^H \mathbf{R}_{\text{dd}}^{-1} \mathbf{y} \\ &= \mathbf{K}_B^H \mathbf{R}_{\text{yy}}^{-1} \mathbf{y} \end{aligned} \quad (23)$$

where the matrix inversion lemma [22] has been used. The corresponding minimum BMSE is [19]:

$$\text{BMSE}_{\text{MMSE}} = \text{trace} \left[(\mathbf{I}_{L_B} + \mathbf{K}_B^H \mathbf{R}_{\text{dd}}^{-1} \mathbf{K}_B)^{-1} \right]. \quad (24)$$

We recall that both the LSE and MLE require that \mathbf{K}_B be full column rank. As discussed in Subsection III-A, such a condition is met if and only if the number of antennas at Alice is not smaller than the number of paths from Bob to Alice and, moreover, the corresponding AoAs are distinct. In contrast, it can be seen from (23) that, in the case at hand, the MMSEE requires the invertibility of $\mathbf{I}_{L_B} + \mathbf{K}_B^H \mathbf{R}_{\text{dd}}^{-1} \mathbf{K}_B$. For this to hold, \mathbf{K}_B need not be full column rank. Therefore, the MMSEE (23) can exist even if $N < L_B$ and/or $\theta_{B,1}, \theta_{B,2}, \dots, \theta_{B,L_B}$ are not distinct. However, under these circumstances, as shown soon after, the performance of the MMSEE (23) is adversely affected by the spoofing attack, even in the absence of noise. The synthesis of (23) requires $\mathcal{O}(N^3)$ flops to invert \mathbf{R}_{yy} .

It is shown in Appendix C that the MMSEE (23) attains the *Bayesian CRLB* [33]. Therefore, since the error of the MMSEE cannot be larger than that of the maximum *a posteriori probability estimator (MAPE)* [33], the MMSEE and MAPE are equal in this case. Similarly to the MLE, the MMSEE (23) can avoid the spoofing attack in the high-SNR region, as stated by the following lemma.

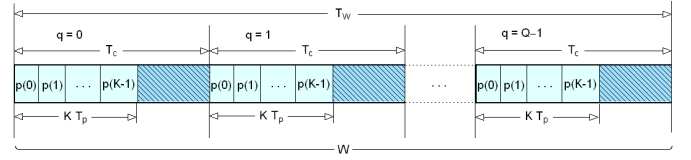


Fig. 2. A specific training design for estimating \mathbf{R}_{yy} .

Lemma 4.1: If the matrix $[\mathbf{A}_B, \mathbf{A}_E] \in \mathbb{C}^{N \times (L_B + L_E)}$ has full column rank, then

$$\overline{\text{BMSE}}_{\text{MMSE}} \triangleq \lim_{\sigma_v^2 \rightarrow 0} \text{BMSE}_{\text{MMSE}} = 0. \quad (25)$$

Proof: See Appendix D. ■

The full-column rank property of $[\mathbf{A}_B, \mathbf{A}_E]$ is a sufficient condition to ensure that the subspaces $\mathcal{R}(\mathbf{A}_B)$ and $\mathcal{R}(\mathbf{A}_E)$ are nonoverlapping (see Subsection III-B). Therefore, both the MLE and MMSEE (23) perfectly reject the spoofing signal in the absence of noise, provide that $\text{rank}([\mathbf{A}_B, \mathbf{A}_E]) = L_B + L_E$. As also pointed out at the end of Subsection III-B, violation of such a condition is unlikely in practice. Moreover, the MMSEE is robust against a partial overlap between the AoA ranges of Bob and Eve (see Section V).

Apart from the knowledge of \mathbf{K}_B , the synthesis of the MMSEE (23) requires estimation of \mathbf{R}_{yy} . Such a correlation matrix is the result of an averaging operation taken over the noise, as well as over the fading vectors \mathbf{h}_B and \mathbf{h}_E . Henceforth, estimation of \mathbf{R}_{yy} requires a dedicated training session – *different from that used to estimate \mathbf{h}_B through (23)* – spanning a time window \mathcal{W} , whose duration T_w is sufficiently larger than the coherence time T_c of the channel. In principle, \mathbf{R}_{yy} can be consistently estimated by the training scheme depicted in Fig. 2. Let T_p be the period of the pilot symbols transmitted by Bob and Eve, the duration T_w can be divided in Q coherence intervals of the channel, i.e., $T_w = Q T_c$, and the number K of pilot symbols \mathbf{p} (the same used to estimate \mathbf{h}_B) can be chosen such that $K T_p = T_c - T_d$, where T_d is the length of the downlink information-bearing session.⁶ If $\mathbf{y}^{(q)} \in \mathbb{C}^N$ denote the data block (8) received by Alice during the q th coherence interval of the channel within \mathcal{W} , for $q \in \{0, 1, \dots, Q-1\}$, the correlation matrix \mathbf{R}_{yy} can be estimated as follows

$$\mathbf{S}_{\text{yy}} \triangleq \frac{1}{Q} \sum_{q=0}^{Q-1} \mathbf{y}^{(q)} [\mathbf{y}^{(q)}]^H. \quad (26)$$

Such a procedure gives a consistent estimate of \mathbf{R}_{yy} , provided that both Bob and Eve transmit during the time window \mathcal{W} the same pilot vector \mathbf{p} used to estimate \mathbf{h}_B through (23). The *sample matrix inversion (SMI)* implementation of the MMSEE (23) is obtained by replacing \mathbf{R}_{yy} in (23) with \mathbf{S}_{yy} , that is

$$\hat{\mathbf{h}}_{B, \text{MMSE-SMI}} = \mathbf{K}_B^H \mathbf{S}_{\text{yy}}^{-1} \mathbf{y} \quad (27)$$

⁶We do not consider uplink data transmissions in our discussion. However, if the legitimate users access the uplink channel in an orthogonal fashion and Eves transmit jamming signals to degrade the reception of the Bobs' data at Alice [18], the estimation accuracy of the correlation matrix \mathbf{R}_{yy} can be further improved by considering uplink data symbols, too.

which might exhibit a severe performance degradation with respect to its ideal counterpart if Q is not sufficiently large.

To mitigate the performance degradation due to finite-sample-size effects, one can resort to the *subspace* implementation of the MMSEE (23), by exploiting the properties of the eigenvalue decomposition (EVD) of $\mathbf{R}_{\mathbf{y}\mathbf{y}}$.⁷ If $[\mathbf{A}_B, \mathbf{A}_E]$ has full column rank (see Lemma 4.1), accounting for (18) and recalling that $\mathbf{R}_{\mathbf{d}\mathbf{d}} = \mathbf{K}_E \mathbf{K}_E^H + \sigma_v^2 \mathbf{I}_N$, the EVD of $\mathbf{R}_{\mathbf{y}\mathbf{y}}$ is given by $\mathbf{R}_{\mathbf{y}\mathbf{y}} = \mathbf{U}_s \mathbf{\Lambda}_s \mathbf{U}_s^H + \sigma_v^2 \mathbf{U}_n \mathbf{U}_n^H$, where $\mathbf{U}_s \in \mathbb{C}^{N \times (L_B + L_E)}$ collects the eigenvectors associated with the $L_B + L_E$ largest eigenvalues $\lambda_1, \lambda_2, \dots, \lambda_{L_B + L_E}$ of $\mathbf{R}_{\mathbf{y}\mathbf{y}}$ (arranged in decreasing order), whose columns span the *signal subspace* corresponding to the Bob and Eve transmissions, i.e., the subspace $\mathcal{R}(\mathbf{K})$ of $\mathbf{K} \triangleq [\mathbf{K}_B, \mathbf{K}_E] \in \mathbb{C}^{N \times (L_B + L_E)}$, while $\mathbf{U}_n \in \mathbb{C}^{N \times (N - L_B - L_E)}$ collects the eigenvectors associated with the eigenvalue σ_v^2 , whose columns span the *noise subspace*, i.e., the orthogonal complement $\mathcal{R}^\perp(\mathbf{K})$ in \mathbb{C}^N of the subspace $\mathcal{R}(\mathbf{K})$ and, finally, $\mathbf{\Lambda}_s \triangleq \text{diag}(\lambda_1, \lambda_2, \dots, \lambda_{L_B + L_E})$. By substituting the EVD of $\mathbf{R}_{\mathbf{y}\mathbf{y}}$ in (18) and exploiting the orthogonality between signal and noise subspaces, one equivalently obtains

$$\hat{\mathbf{h}}_{B, \text{MMSE}} = \mathbf{K}_B^H \mathbf{U}_s \mathbf{\Lambda}_s^{-1} \mathbf{U}_s^H \mathbf{y}. \quad (28)$$

Since in practice the EVD is performed on $\mathbf{S}_{\mathbf{y}\mathbf{y}}$ given by (26), by denoting the sample matrices corresponding to \mathbf{U}_s and $\mathbf{\Lambda}_s$ with $\hat{\mathbf{U}}_s$ and $\hat{\mathbf{\Lambda}}_s$, respectively, one has

$$\hat{\mathbf{h}}_{B, \text{MMSE-SUB}} = \mathbf{K}_B^H \hat{\mathbf{U}}_s \hat{\mathbf{\Lambda}}_s^{-1} \hat{\mathbf{U}}_s^H \mathbf{y}. \quad (29)$$

It is noteworthy that the estimator (29) is not equal to (27), since $\mathbf{K}_B^H \hat{\mathbf{U}}_n \neq \mathbf{O}_{L_B \times (N - L_B - L_E)}$ due to the finite-sample size effects, where $\hat{\mathbf{U}}_n$ being the sample matrix of \mathbf{U}_n . This implies that (27) and (29) might exhibit different BMSE performances (see Subsection V-C). The estimator (29) basically demands the same computational burden as (27) and, additionally, requires the knowledge of the dimension $L_B + L_E$ of the signal subspace, which can be obtained from $\mathbf{S}_{\mathbf{y}\mathbf{y}}$ by using the minimum description length criterion [36].

B. Case 2: Imperfect knowledge of \mathbf{K}_E

Herein, our aim is to study the impact on the system performance of errors regarding the knowledge of the transmission parameters of Eve. Starting from an estimate of $\mathbf{R}_{\mathbf{d}\mathbf{d}}$ or, equivalently, $\mathbf{R}_{\mathbf{y}\mathbf{y}}$, ML/MAP estimators [37] or other computationally simpler subspace-based estimation procedures [38], [39] can be used to estimate \mathbf{K}_E . Therefore, we assume that estimates of the AoAs and the average transmit power of Eve are available at Alice, which are expressed [40], [41] as⁸

$$\hat{\theta}_{E, \ell} = \theta_{E, \ell} + \Delta\theta_{E, \ell}, \quad \text{for } \ell \in \{1, 2, \dots, L_E\} \quad (30)$$

$$\hat{\mathcal{P}}_E = \mathcal{P}_E e^{\Delta\mathcal{P}_E} \quad (31)$$

⁷Another viable alternative is represented by shrinkage-based methods, which have the potential to enhance the performance of correlation matrix estimation with small number of samples [35].

⁸For the sake of analysis, we assume in Case 2 that the number L_E of paths between Eve and Alice are also known. In practice, an upper bound of L_E might be available since, depending on the transmitted signal parameters (carrier frequency and bandwidth) and application (indoor or outdoor), the maximum channel multipath spread may be known *a priori*.

where $\hat{\theta}_{E, \ell}$ and $\hat{\mathcal{P}}_E$ are estimates of $\theta_{E, \ell}$ and \mathcal{P}_E , respectively, whereas the random variables (see Appendix E)

$$\Delta\theta_{E, \ell} \sim \mathcal{N}_T(0, \sigma_{\theta_E}, -\Delta\theta_{E, \max}, \Delta\theta_{E, \max}) \quad (32)$$

$$\Delta\mathcal{P}_E \sim \mathcal{N}_T(0, \sigma_{\mathcal{P}_E}, -\Delta\mathcal{P}_{E, \max}, \Delta\mathcal{P}_{E, \max}) \quad (33)$$

denote the corresponding errors that model the *uncertainty* on the knowledge of the spoofing transmission parameters. It is also assumed that $\Delta\theta_{E, 1}, \Delta\theta_{E, 2}, \dots, \Delta\theta_{E, L_E}$, and $\Delta\mathcal{P}_E$ are mutually independent random variables, statistically independent of the triple $(\mathbf{h}_B, \mathbf{h}_E, \mathbf{v})$, whose probability distributions are known at Alice, along with the noise variance σ_v^2 (see Subsection III-B for a brief discussion about such an assumption). As shown in Appendix E, the random variable $e^{\Delta\mathcal{P}_E}$ in (31) has a truncated lognormal distribution.

In this case, the optimal MMSEE minimizes the BMSE (9), where the average is taken not only over $(\mathbf{h}_B, \mathbf{h}_E, \mathbf{v})$, but over the pdf of $(\Delta\theta_{E, 1}, \Delta\theta_{E, 2}, \dots, \Delta\theta_{E, L_E}, \Delta\mathcal{P}_E)$, too. This estimator is *not* linear: it is difficult to determine in closed form and its computational complexity is prohibitive in practice. Two mathematically tractable solutions are reported in the following subsections by retaining the Bayesian MMSE criterion but constraining the estimators to be *linear*.

1) *Naive LMMSEE*: As a first strategy to synthesize a LMMSEE [19] with affordable complexity, Alice can disregard the knowledge of the statistics of $\Delta\theta_{E, 1}, \Delta\theta_{E, 2}, \dots, \Delta\theta_{E, L_E}, \Delta\mathcal{P}_E$ and simply build the estimate $\hat{\mathbf{K}}_E \triangleq \sqrt{\hat{\mathcal{P}}_E} \hat{\mathbf{A}}_E$ of \mathbf{K}_E , where $\hat{\mathbf{A}}_E$ is obtained from \mathbf{A}_E by replacing $\theta_{E, \ell}$ with $\hat{\theta}_{E, \ell}$, for $\ell \in \{1, 2, \dots, L_E\}$. So doing, an approximated version of (23) is developed as

$$\hat{\mathbf{h}}_{B, \text{LMMSE}}^{(1)} = \mathbf{K}_B^H \hat{\mathbf{R}}_{\mathbf{y}\mathbf{y}}^{-1} \mathbf{y} \quad (34)$$

with $\hat{\mathbf{R}}_{\mathbf{y}\mathbf{y}} \triangleq \mathbf{K}_B \mathbf{K}_B^H + \hat{\mathbf{K}}_E \hat{\mathbf{K}}_E^H + \sigma_v^2 \mathbf{I}_N$. In this case, the corresponding BMSE can be calculated by substituting (34) in (9) and, by virtue of the conditional expectation rule [42], further averaging the obtained result with respect to the pdf of $(\Delta\theta_{E, 1}, \Delta\theta_{E, 2}, \dots, \Delta\theta_{E, L_E}, \Delta\mathcal{P}_E)$. So doing, one has

$$\begin{aligned} \text{BMSE}_{\text{LMMSE}}^{(1)} &\triangleq \mathbb{E} \left\{ \text{trace} \left[\mathbf{K}_B^H \hat{\mathbf{R}}_{\mathbf{y}\mathbf{y}}^{-1} \left(\mathbf{R}_{\mathbf{y}\mathbf{y}} \hat{\mathbf{R}}_{\mathbf{y}\mathbf{y}}^{-1} - \mathbf{I}_N \right) \mathbf{K}_B \right] \right\} \\ &+ \mathbb{E} \left\{ \text{trace} \left[\left(\mathbf{I}_{L_B} + \mathbf{K}_B^H \hat{\mathbf{R}}_{\mathbf{d}\mathbf{d}}^{-1} \mathbf{K}_B \right)^{-1} \right] \right\} \quad (35) \end{aligned}$$

with $\hat{\mathbf{R}}_{\mathbf{d}\mathbf{d}} \triangleq \hat{\mathbf{K}}_E \hat{\mathbf{K}}_E^H + \sigma_v^2 \mathbf{I}_N$. We have numerically verified that the predominant cause of BMSE degradation is represented by the first summand in (35) and, thus, replacing $\hat{\mathbf{R}}_{\mathbf{d}\mathbf{d}}$ with $\mathbf{R}_{\mathbf{d}\mathbf{d}}$ in (35) has a very marginal effect on $\text{BMSE}_{\text{LMMSE}}^{(1)}$. Therefore, remembering (24), we get

$$\text{BMSE}_{\text{LMMSE}}^{(1)} \approx \text{BMSE}_{\text{MMSE}} + \Delta\text{BMSE}_{\text{LMMSE}}^{(1)} \quad (36)$$

with

$$\Delta\text{BMSE}_{\text{LMMSE}}^{(1)} \triangleq \mathbb{E} \left\{ \text{trace} \left[\mathbf{K}_B^H \hat{\mathbf{R}}_{\mathbf{y}\mathbf{y}}^{-1} \left(\mathbf{R}_{\mathbf{y}\mathbf{y}} \hat{\mathbf{R}}_{\mathbf{y}\mathbf{y}}^{-1} - \mathbf{I}_N \right) \mathbf{K}_B \right] \right\}. \quad (37)$$

It is apparent from (37) that, in the low-SNR regime, i.e., when σ_v^2 is sufficiently large compared to the maximum eigenvalue of $\mathbf{K}_B \mathbf{K}_B^H$, $\mathbf{K}_E \mathbf{K}_E^H$, and $\hat{\mathbf{K}}_E \hat{\mathbf{K}}_E^H$, one has $\hat{\mathbf{R}}_{\mathbf{y}\mathbf{y}} \approx \mathbf{R}_{\mathbf{y}\mathbf{y}} \approx \sigma_v^2 \mathbf{I}_N$ and, thus, $\Delta\text{BMSE}_{\text{LMMSE}}^{(1)} \approx 0$. On the other hand, for

TABLE I
SYSTEM KNOWLEDGE AND COMPUTATIONAL COMPLEXITY OF THE
CONSIDERED CHANNEL ESTIMATORS

Estimator	System Knowledge	Complexity (flops)
LSE (11)	\mathbf{K}_B (full-column rank)	$\mathcal{O}(L_B^3)$
MLE (17)	\mathbf{K}_B (full-column rank), \mathbf{R}_{dd}	$\mathcal{O}(N^3)$
MMSEE (23)	$\mathbf{K}_B, \mathbf{R}_{yy}$	$\mathcal{O}(N^3)$
LMMSEE (34)	$\mathbf{K}_B, \{\hat{\theta}_{E,\ell}\}_{\ell=1}^{L_E}, \hat{\mathcal{P}}_E, \sigma_v^2$	$\mathcal{O}(N^3)$
LMMSEE (38)	$\mathbf{K}_B, \{\hat{\theta}_{E,\ell}\}_{\ell=1}^{L_E}, \hat{\mathcal{P}}_E, \sigma_v^2$, pdf of $\{\Delta\theta_{E,\ell}\}_{\ell=1}^{L_E}$ and $\Delta\mathcal{P}_E$	$\mathcal{O}(N^3)$

high SNR values, i.e., when σ_v^2 is sufficiently small compared to the minimum eigenvalue of $\mathbf{K}_B \mathbf{K}_B^H$, $\mathbf{K}_E \mathbf{K}_E^H$, and $\hat{\mathbf{K}}_E \hat{\mathbf{K}}_E^H$, it results that $\mathbf{R}_{yy} \neq \hat{\mathbf{R}}_{yy}$, which implies that $\Delta\text{BMSE}_{\text{LMMSE}}^{(1)}$ might be nonzero. In summary, errors regarding the knowledge of the Eve's parameters may be deleterious at the high-SNR regime, whereas they are nearly irrelevant for low SNR values.

2) *Improved LMMSEE*: An alternative design can be pursued by additionally making use of the statistics of $\Delta\theta_{E,1}, \Delta\theta_{E,2}, \dots, \Delta\theta_{E,L_E}, \Delta\mathcal{P}_E$. In this case, the structure of the LMMSEE is derived in Appendix F and it reads as shown in (38) at the top of the next page, with

$$\mathbb{E}[e^{-\Delta\mathcal{P}_E}] = \frac{e^{-\frac{\sigma_{\mathcal{P}_E}^2}{2}}}{2 \operatorname{erf}\left(\frac{\Delta\mathcal{P}_{E,\max}}{\sqrt{2}\sigma_{\mathcal{P}_E}}\right)} \left[\operatorname{erf}\left(\frac{\Delta\mathcal{P}_{E,\max} - \sigma_{\mathcal{P}_E}^2}{\sqrt{2}\sigma_{\mathcal{P}_E}}\right) + \operatorname{erf}\left(\frac{\Delta\mathcal{P}_{E,\max} + \sigma_{\mathcal{P}_E}^2}{\sqrt{2}\sigma_{\mathcal{P}_E}}\right) \right] \quad (39)$$

whereas the (n_1+1, n_2+1) th entry of $\mathbf{R}_{aa}^{(\ell)}$ is reported in (40) at the top of the next page, for $n_1, n_2 \in \{0, 1, \dots, N-1\}$.

The synthesis of (38) essentially requires the same complexity of (23) and (34). The estimator (38) exploits the prior information on the estimation error of the Eve's parameters to outperform the naive LMMSE, especially for moderate-to-high SNR values. Its performance will be numerically evaluated in the forthcoming Section V.

V. NUMERICAL RESULTS

Tab. I reports the system information required for calculating the considered estimators and the corresponding computation complexity. The performance analysis of such estimators was developed by resorting to Monte Carlo simulations in order to corroborate our theoretical findings as well. To this aim, we considered the following simulation setting. The number of antennas at Alice is set equal to $N = 10$, with an absolute antenna spacing $d = \lambda_c/2$. With reference to the multi-user scenario depicted in Fig. 1, we considered two Bob-Eve pairs, i.e., $M = 2$. The number of Bob-to-Alice and Eve-to-Alice paths was chosen equal to $L_{B,1} = L_{E,1} = 3$ for the first Bob-Eve pair, whereas $L_{B,2} = L_{E,2} = 2$ for the second one. The AoAs of Bob 1 and Bob 2 were fixed as follows: $\theta_{B,1,1} = 0$, $\theta_{B,2,1} = \psi$, $\theta_{B,3,1} = \pi/5$, $\theta_{B,1,2} = (3/5)\pi$, and $\theta_{B,2,2} = (7/10)\pi$, respectively, with the parameter $\psi \in [0, \pi/10]$. It should be observed that, when $\psi \rightarrow 0$, the

matrix $\mathbf{K}_{B,1}$ tends to lose its full column rank property. On the other hand, the AoAs of Eve 1 and Eve 2 were chosen as: $\theta_{E,1,1} = \pi/5 + \phi$, $\theta_{E,2,1} = (2/5)\pi$, $\theta_{E,3,1} = \pi/2$, $\theta_{E,1,2} = (4/5)\pi$, and $\theta_{E,2,2} = (9/10)\pi$, respectively, with the parameter $\phi \in [0, \pi/10]$. It is noteworthy that, when $\phi \rightarrow 0$, the columns of $\mathbf{A}_{B,1}$ and $\mathbf{A}_{E,1}$ become linearly dependent. The pilot vectors \mathbf{p}_1 and \mathbf{p}_2 were obtained by picking two different columns of a unitary K -point discrete Fourier transform matrix, with $K = 8$. Unless otherwise specified, we set $\psi = \phi = \pi/10$, $\text{SNR}_B \triangleq \mathcal{P}_{B,1}/\sigma_v^2 = \mathcal{P}_{B,2}/\sigma_v^2 = 30$ dB, $\text{SSR} \triangleq \mathcal{P}_{B,1}/\mathcal{P}_{E,1} = \mathcal{P}_{B,2}/\mathcal{P}_{E,2} = 0$ dB, $\sigma_{\theta_E} = \Delta\theta_{E,\max}/3$, $\Delta\theta_{E,\max} = \pi/25$ (corresponding to a interval of uncertainty $2\Delta\theta_{E,\max}$ of 0.08π rad), $\sigma_{\mathcal{P}_E} = \Delta\mathcal{P}_{E,\max}/2$, $\Delta\mathcal{P}_{E,\max} = 0.3454$ (corresponding to a interval of uncertainty $2\Delta\mathcal{P}_{E,\max}$ of 3 dB), and we implemented the MLE (17) and MMSEE (23) by using the exact expression of \mathbf{R}_{dd} and \mathbf{R}_{yy} .

Two performance metrics were used to evaluate the channel estimation performance of the first legitimate user. The former is a *normalized* version of the BMSE defined in (9):

$$\text{NBMSE}(\hat{\mathbf{h}}_{B,1}) \triangleq \mathbb{E} \left[\frac{\|\hat{\mathbf{h}}_{B,1} - \mathbf{h}_{B,1}\|^2}{\|\mathbf{h}_{B,1}\|^2} \right]. \quad (41)$$

The latter is the achievable (*ergodic*) *secrecy rate* [43] of the downlink transmission from Alice to Bob 1:

$$\mathcal{C}_s \triangleq \max(\mathcal{C}_{B,1} - \mathcal{C}_{E,1}, 0) \quad (42)$$

where, for $\text{RX} \in \{B, E\}$,

$$\mathcal{C}_{\text{RX},1} = \mathbb{E}[\log_2(1 + \text{SINR}_{\text{RX},1})] \quad (43)$$

is the maximum achievable *normalized*⁹ (ergodic) spectral efficiency (in bits/s/Hz) of the Alice-to-RX downlink channel,

$$\text{SINR}_{\text{RX},1} \triangleq \frac{\text{SNR}_{\text{DL}} |\mathbf{h}_{\text{RX},1}^T \mathbf{A}_{\text{RX},1}^T \mathbf{w}_1|^2}{\text{SNR}_{\text{DL}} \sum_{m=2}^M |\mathbf{h}_{\text{RX},1}^T \mathbf{A}_{\text{RX},1}^T \mathbf{w}_m|^2 + 1} \quad (44)$$

denotes the corresponding signal-to-interference-plus-noise ratio (SINR) under the assumption that the Alice transmits independent and identically distributed zero-mean unit-variance symbols, with SNR_{DL} representing the SNR (assumed to be independent of m) and $\mathbf{W} \triangleq [\mathbf{w}_1, \mathbf{w}_2, \dots, \mathbf{w}_M] \in \mathbb{C}^{N \times M}$ being the precoding matrix at Alice. We considered the unit-norm matched-filter precoder [44], which is given by $\mathbf{W} = \hat{\mathbf{H}}_B^* / \|\hat{\mathbf{H}}_B\|$, with $\hat{\mathbf{H}}_B \triangleq [\mathbf{A}_{B,1} \hat{\mathbf{h}}_{B,1}, \mathbf{A}_{B,2} \hat{\mathbf{h}}_{B,2}, \dots, \mathbf{A}_{B,M} \hat{\mathbf{h}}_{B,M}]$. As a reference, we also reported the performance of the estimators (11), (17), and (23) when the Eves do not attack the pilot session of the legitimate users, i.e., $\mathcal{P}_{E,m} = 0$, $\forall m \in \mathcal{M}$, and, thus, they steal information in downlink only, referred to as “passive Eves”. In this respect, it should be observed that $\mathbf{R}_{dd} = \sigma_v^2 \mathbf{I}_N$ and, thus, the MLE (17) ends up to the LSE (11). Finally, all the results are obtained by carrying out 10^5 independent Monte Carlo trials, with each run using different sets of channel coefficients and noise.

⁹The normalization by the factor T_d/T_c was introduced for convenience, where we remember that T_d is the length of the downlink data session and T_c is the channel coherence time.

$$\hat{\mathbf{h}}_{B, \text{LMMSE}}^{(2)} = \mathbf{K}_B^H \left\{ \mathbf{K}_B \mathbf{K}_B^H + \hat{\mathcal{P}}_E \mathbb{E} [e^{-\Delta \mathcal{P}_E}] \frac{1}{L_E} \sum_{\ell=1}^{L_E} \mathbf{R}_{\text{aa}}^{(\ell)} + \sigma_v^2 \mathbf{I}_N \right\}^{-1} \mathbf{y} \quad (38)$$

$$\left\{ \mathbf{R}_{\text{aa}}^{(\ell)} \right\}_{n_1+1, n_2+1} = \frac{1}{N} \left\{ 1 - \left[4\pi^2 (n_1 - n_2)^2 \Delta^2 \sin^2(\hat{\theta}_{E, \ell}) - j 2\pi (n_1 - n_2) \Delta \cos(\hat{\theta}_{E, \ell}) \right] \sigma_{\theta_E}^2 \right. \\ \left. \cdot \left[\frac{1}{2} - \frac{\Delta \theta_{E, \max}}{\text{erf} \left(\frac{\Delta \theta_{E, \max}}{\sqrt{2} \sigma_{\theta_E}} \right) \sqrt{2\pi} \sigma_{\theta_E}} e^{-\frac{\Delta \theta_{E, \max}^2}{2\sigma_{\theta_E}^2}} \right] \right\} e^{-j[2\pi (n_1 - n_2) \Delta \cos(\hat{\theta}_{E, \ell})]} \quad (40)$$

A. Example 1 : Performance as a function of SNR_B

In this subsection, we reported the performance of the considered channel estimators as a function of SNR_B , ranging from 0 to 34 dB. Results of Fig. 3 confirm that the LSE is unable to counteract the pilot spoofing attack, by showing the BMSE floor predicted by Lemma 3.1. On the other hand, according to Lemmas 3.2 and 4.1, the MLE and MMSEE are able to suppress the pilot spoofing signal in the high- SNR_B region, by exhibiting almost the same performance of the corresponding estimators in the absence of the pilot spoofing attack. The performance of the naive LMMSE gets worse for increasing values of SNR_B , due to the presence of the summand $\Delta \text{BMSE}_{\text{LMMSE}}^{(1)}$ in (37). Such a negative effect is compensated for by exploiting the knowledge of the estimation error of the Eves' parameters, as testified by the satisfactory asymptotic (i.e., for $\text{SNR}_B \rightarrow +\infty$) performance of the improved LMMSE.

B. Example 2: Performance as a function of SSR

We depicted in Fig. 4 the performance of the considered channel estimators as a function of the SSR, ranging from -10 to 20 dB. Besides confirming that, for high SNR values, the performance of the MLE and MMSEE is almost unaffected by the pilot spoofing attack, independently of the value of the SSR, it is apparent that the channel estimation accuracy of the LSE becomes acceptable only for high SSR values. It is also interesting to note that the performance of the naive LMMSE rapidly worsens as the SSR decreases, while the improved LMMSE exhibits a spoofing-resistant capability for a wider range of SSR values.

C. Example 3: Performance of the MMSEE with sample correlation matrix \mathbf{S}_{yy}

To show how much training is needed to reliably estimate \mathbf{R}_{yy} according to the training protocol reported in Fig. 2, we plotted in Fig. 5 the performance of the MMSEE as a function of Q . As expected, the SMI implementation (27) requires a huge number Q of channel coherence intervals for achieving satisfactory performance, whereas its subspace counterpart (29) converges to the ideal BMSE (24) much more quickly, by ensuring a reduction of the length of the time window \mathcal{W} of about one order of magnitude. Similar conclusions apply to the MLE as well, when it is implemented starting from \mathbf{S}_{dd} .

D. Example 4: Performance as a function of ψ and ϕ

We depicted in Fig. 6 the performance of the considered channel estimators as a function of ψ . When $\psi \rightarrow 0$, the condition $\text{rank}(\mathbf{K}_B) = L_B$ tends to be violated. The non-fulfillment of such a rank condition does not prevent the MLE, MMSEE, and LMMSEs to satisfactorily estimate the legitimate channel, although perfect cancellation of the pilot spoofing signal at high SNR values is not ensured anymore.

We also studied the impact of ϕ on the performance of the considered channel estimators. Results of Fig. 7 show that the MLE, MMSEE, and LMMSEs exhibit a certain robustness when the legitimate and the spoofing transmissions tend to have a common AoA, i.e., when $\phi \rightarrow 0$, and, thus, the columns of \mathbf{A}_B and \mathbf{A}_E are no longer linearly independent.

E. Example 5: Performance as a function of σ_{θ_E}

Finally, we investigated the performance of the LMMSEs derived in Subsection IV-B as a function of the standard deviation σ_{θ_E} , with $\Delta \theta_{E, \max} = \pi/(25)$.¹⁰ It can be seen from Fig. 8 that the performance of the LMMSEs gracefully degrades as the uncertainty on the knowledge of the spoofing AoAs increases, by enlightening that even an imperfect knowledge of the spoofing transmission parameters can lead to a significant performance gain with respect to the simpler LSE.

VI. CONCLUSIONS AND DIRECTIONS FOR FUTURE WORK

Five uplink channel estimation schemes for multiple antennas systems have been developed and studied in the case of a pilot spoofing attack, namely, LSE, MLE, MMSEE, naive and improved LMMSEs. The LSE does not require knowledge of the statistics of the legitimate channel or the correlation matrix of the spoofing-plus-noise signal and, hence, it does not have any spoofing suppression capability. On the other hand, compared to the LSE, the MLE has better accuracy as it involves the correlation matrix of the spoofing-plus-noise signal. At low SNR, a performance gain over the MLE is ensured by the MMSEE, since it additionally incorporates the statistics of the legitimate channel. The naive LMMSEE can be designed if an estimate of the main spoofing parameters is available, whereas the improved LMMSEE also exploits prior information regarding the estimation error.

¹⁰Results – not reported here for the sake of brevity – show that the performance of the LMMSEs are weakly affected by the error on the estimate of the Eve's average transmission power \mathcal{P}_E .

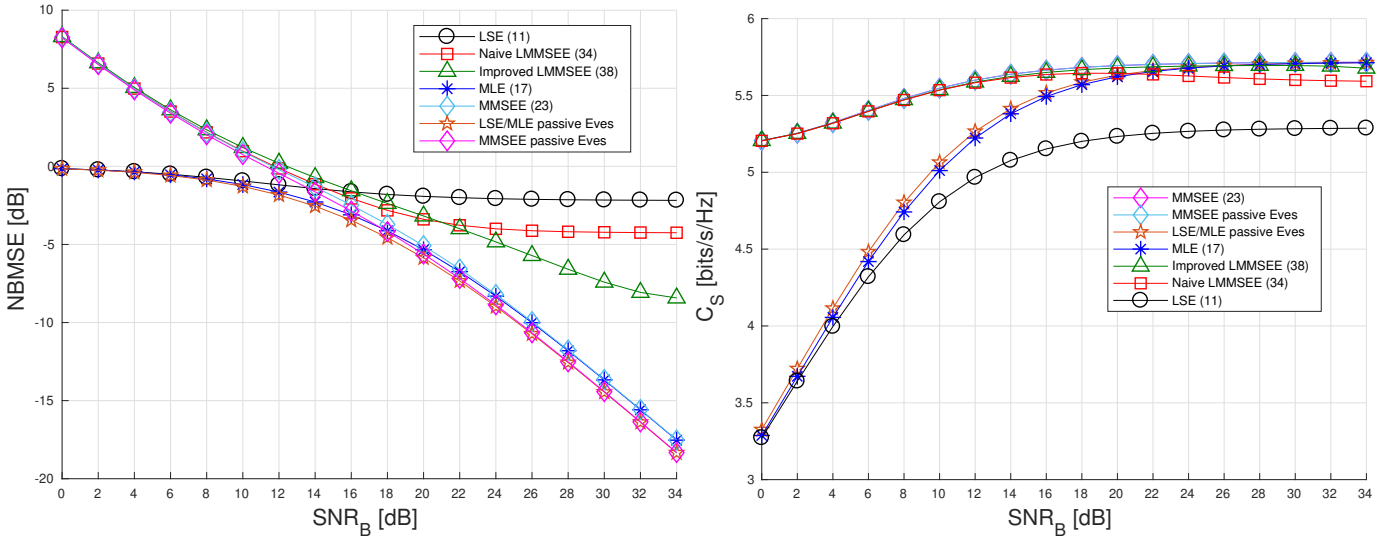
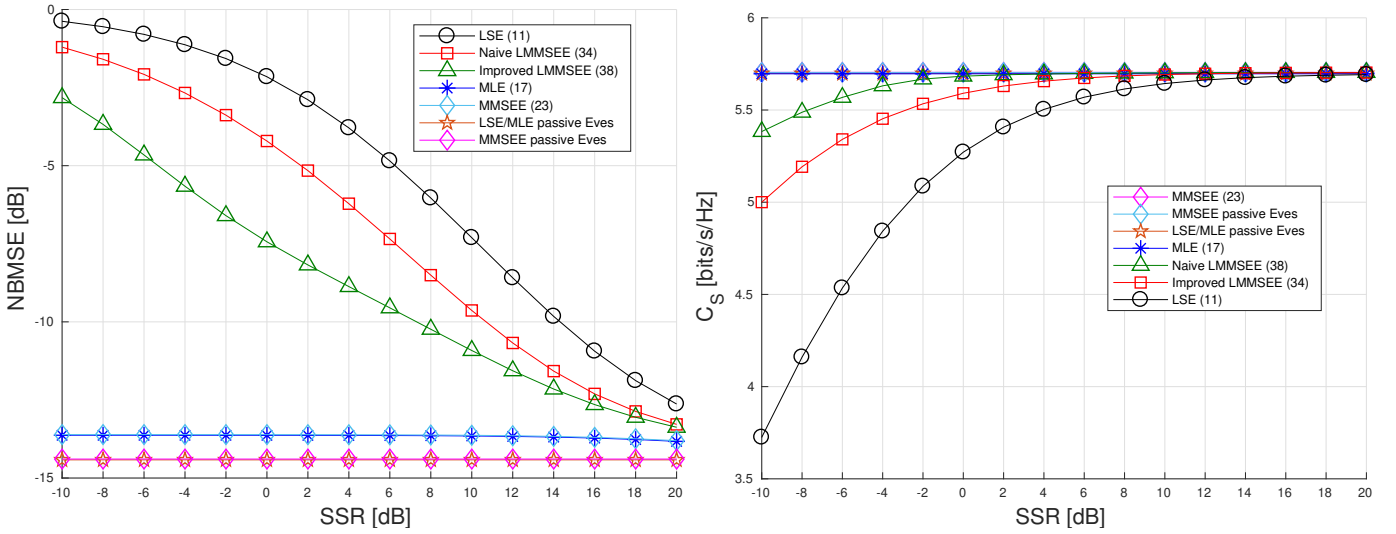
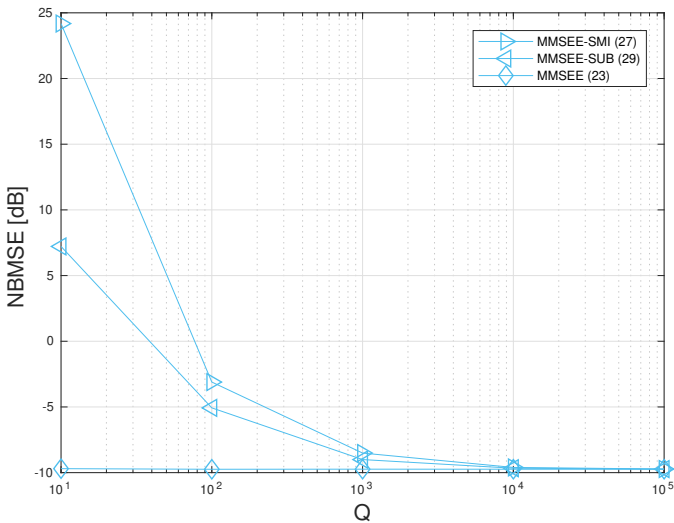
Fig. 3. NBMSE (left) and secrecy rate (right) versus SNR_B (Example 1).

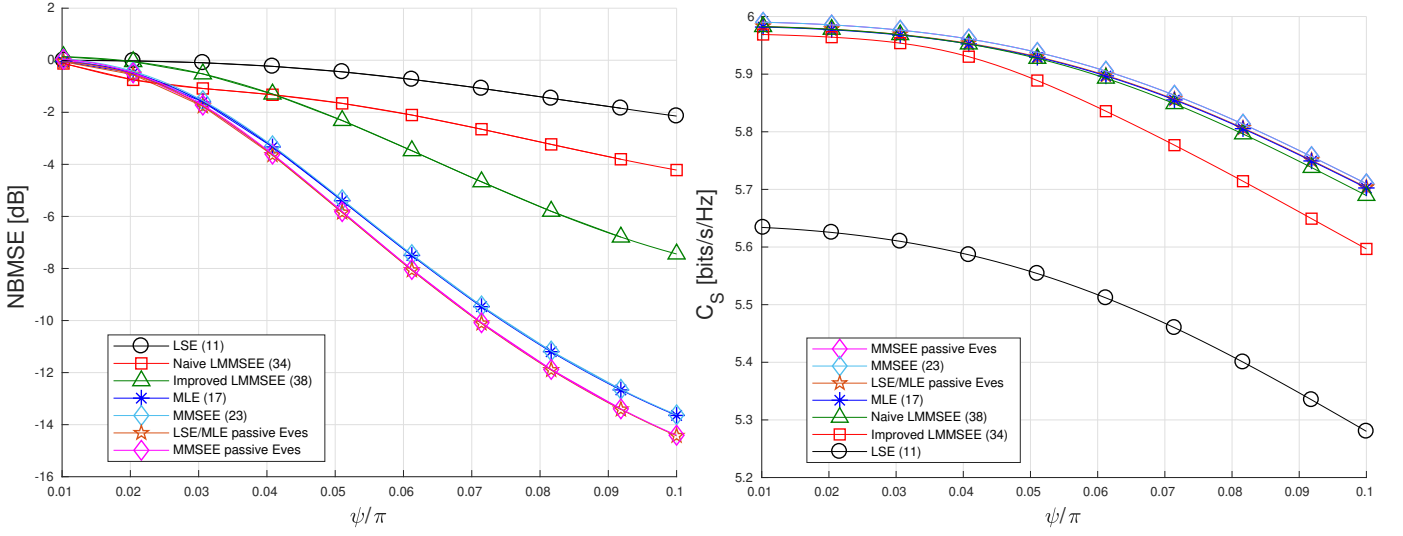
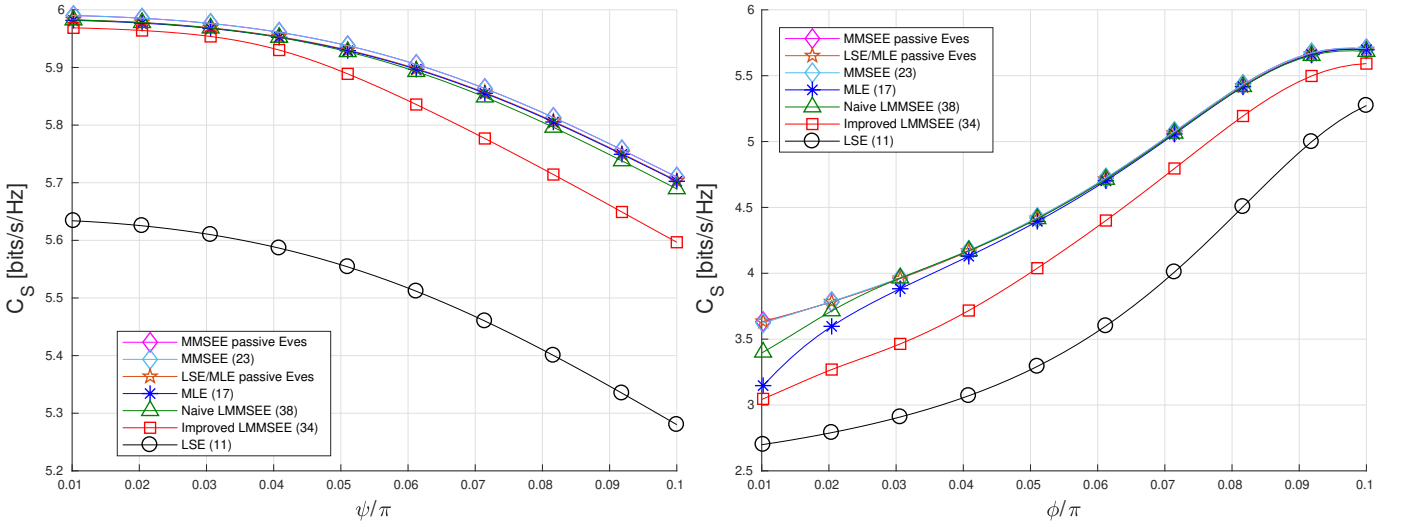
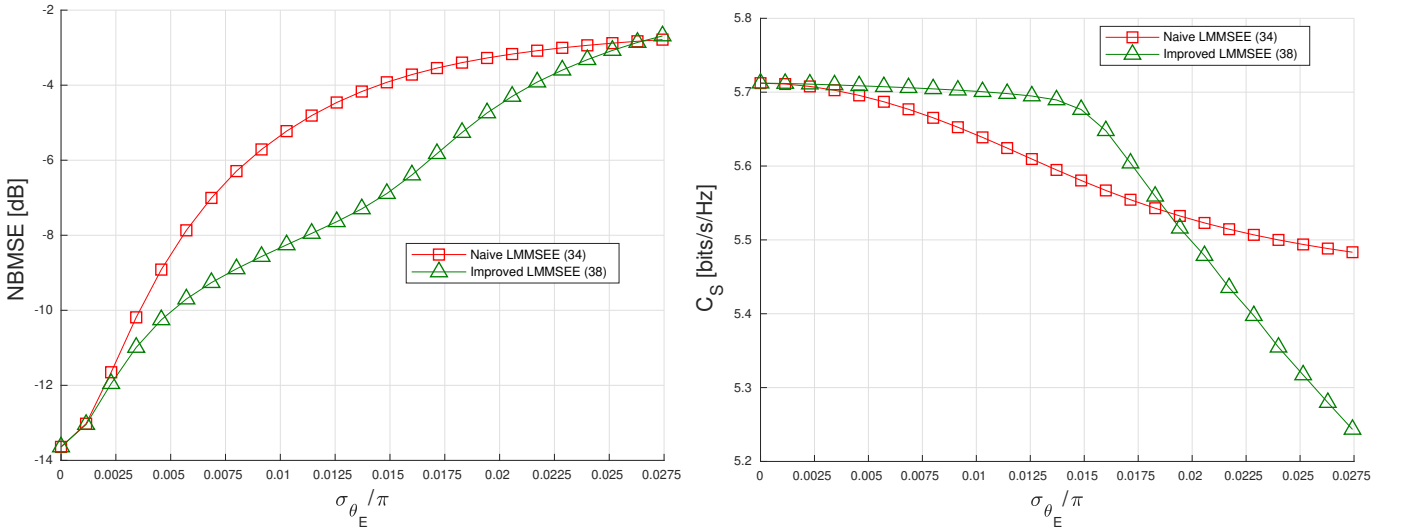
Fig. 4. NBMSE (left) and secrecy rate (right) versus SSR (Example 2).

Fig. 5. NBMSE versus Q (Example 3).

Specifically, the following main results have been found:

- i) Under certain operative conditions, the MLE and MMSEE can be capable of perfectly rejecting the pilot spoofing signal in the high-SNR regime.
- ii) Both the MLE and MMSEE can be entirely implemented from data, but a training session spanning multiple channel coherence intervals is required in a setup phase.
- iii) The estimation error of the spoofing AoAs mainly affects the performance of the naive LMMSEE at high SNR.
- iv) The improved LMMSEE largely outperforms the LSE and the naive LMMSEE even for low SSR values.

In summary, this study demonstrates that, if more sophisticated channel estimators than the LSE are employed, an uplink pilot spoofing attack might be effectively counteracted at the base station, resulting in a very limited signal leakage to Eve in the downlink data phase. Finally, we assumed that a ULA is used at the BS and focused on single-antenna legitimate users. To improve physical-layer security, a viable strategy

Fig. 6. NBMSE (left) and secrecy rate (right) versus ψ (Example 4).Fig. 7. NBMSE (left) and secrecy rate (right) versus ϕ (Example 4).Fig. 8. NBMSE (left) and secrecy rate (right) versus σ_{θ_E} (Example 5).

is to exploit additional spatial dimensions. In this respect, a first interesting research subject consists of considering three-dimensional (or full-dimensional) MIMO at the BS and user terminals equipped with multiple antennas. Moreover, the effects of uplink channel estimation errors on the downlink secrecy rate were studied through numerical simulations. An additional research issue is to develop a theoretical analysis of the downlink SINR that explicitly accounts for both correlation matrix and channel estimation effects. When the legitimate users employ non-orthogonal pilot sequences, it will be also interesting to study the joint effects of pilot spoofing attacks and pilot contamination on uplink channel estimation and downlink secrecy rate.

APPENDIX A PROOF OF LEMMA 3.1

First, we observe that $\mathbf{A}_B (\mathbf{A}_B^H \mathbf{A}_B)^{-2} \mathbf{A}_B^H$ and $\mathbf{A}_E \mathbf{A}_E^H$ are positive semidefinite Hermitian matrices. For positive semidefinite Hermitian matrices $\mathbf{A} \in \mathbb{C}^{n \times n}$ and $\mathbf{B} \in \mathbb{C}^{n \times n}$, with eigenvalues sorted decreasingly $a_1 \geq a_2 \geq \dots \geq a_n$ and $b_1 \geq b_2 \geq \dots \geq b_n$, respectively, it results [45] that

$$\sum_{i=1}^n a_i b_{n-i+1} \leq \text{trace}(\mathbf{A} \mathbf{B}) \leq \sum_{i=1}^n a_i b_i. \quad (45)$$

Therefore, the bound (14) comes from recalling the facts [23] that: (i) the two matrices $\mathbf{A}_B (\mathbf{A}_B^H \mathbf{A}_B)^{-2} \mathbf{A}_B^H$ and $(\mathbf{A}_B^H \mathbf{A}_B)^{-1}$ have the same nonzero eigenvalues; (ii) the singular values $\sigma_\ell(\mathbf{A}_B)$ and $\sigma_\ell(\mathbf{A}_E)$ are the nonnegative square roots of the eigenvalues of $\mathbf{A}_B \mathbf{A}_B^H$ and $\mathbf{A}_E \mathbf{A}_E^H$, respectively.

APPENDIX B PROOF OF LEMMA 3.2

By virtue of the matrix inversion lemma [22], one has

$$\begin{aligned} \mathbf{R}_{dd}^{-1} &= (\mathbf{K}_E \mathbf{K}_E^H + \sigma_v^2 \mathbf{I}_N)^{-1} \\ &= \frac{1}{\sigma_v^2} \left[\mathbf{I}_N - \mathbf{K}_E (\mathbf{K}_E^H \mathbf{K}_E + \sigma_v^2 \mathbf{I}_{L_E})^{-1} \mathbf{K}_E^H \right]. \end{aligned} \quad (46)$$

By substituting (46) in (19) and resorting again to the matrix inversion lemma, one gets

$$\begin{aligned} \text{BMSE}_{\text{ML}} &= \sigma_v^2 \text{trace} \left[(\mathbf{K}_B^H \mathbf{K}_B)^{-1} \right] \\ &+ \sigma_v^2 \text{trace} \left[\mathbf{K}_B^\dagger \mathbf{K}_E (\mathbf{K}_E^H \mathbf{P}_B \mathbf{K}_E + \sigma_v^2 \mathbf{I}_{L_E})^{-1} \mathbf{K}_E^H (\mathbf{K}_B^H)^\dagger \right] \end{aligned} \quad (47)$$

where $\mathbf{P}_B \triangleq \mathbf{I}_N - \mathbf{K}_B (\mathbf{K}_B^H \mathbf{K}_B)^{-1} \mathbf{K}_B^H \in \mathbb{C}^{N \times N}$ is the orthogonal projector onto $\mathcal{N}(\mathbf{K}_B^H)$. We recall that $\mathcal{N}(\mathbf{K}_B^H)$ is the orthogonal complement of $\mathcal{R}(\mathbf{K}_B)$ in \mathbb{C}^N .

It is apparent from (47) that, if $\mathbf{K}_E^H \mathbf{P}_B \mathbf{K}_E = \mathbf{O}_{L_E \times L_E}$, i.e., $\mathcal{R}(\mathbf{K}_E) \subseteq \mathcal{R}(\mathbf{K}_B)$, then

$$\overline{\text{BMSE}}_{\text{ML}} = \text{trace} \left[\mathbf{K}_B^\dagger \mathbf{K}_E \mathbf{K}_E^H (\mathbf{K}_B^H)^\dagger \right] \neq 0 \quad (48)$$

that is, in the absence of noise, the BMSE of the MLE exhibits a saturation effect due to the concurrent spoofing transmission. On the other hand, if $\mathcal{R}(\mathbf{K}_E) \subseteq \mathcal{R}^\perp(\mathbf{K}_B)$ or, equivalently, $\mathcal{R}(\mathbf{K}_B) \cap \mathcal{R}(\mathbf{K}_E) = \{\mathbf{0}_{KN}\}$, one has $\mathbf{K}_B^\dagger \mathbf{K}_E = \mathbf{O}_{L_B \times L_E}$ and,

hence, $\overline{\text{AMSE}}_{\text{ML}} = 0$: in this case, in the absence of noise, perfect spoofing suppression is achieved. As a final step, we observe that the condition $\mathcal{R}(\mathbf{K}_B) \cap \mathcal{R}(\mathbf{K}_E) = \{\mathbf{0}_N\}$ is equivalent to $\mathcal{R}(\mathbf{A}_B) \cap \mathcal{R}(\mathbf{A}_E) = \{\mathbf{0}_N\}$.

APPENDIX C

CASE 1: EVALUATION OF THE BAYESIAN CRLB

Let $p(\mathbf{y}, \mathbf{h}_B)$ be the *joint* pdf of \mathbf{y} and \mathbf{h}_B , under regularity conditions that are satisfied by Gaussian random vectors [33], [34], the *Bayesian information matrix (BIM)* is defined as

$$\mathcal{B} \triangleq \mathbb{E}_{\mathbf{y}, \mathbf{h}_B} \left\{ \frac{\partial \ln p(\mathbf{y}, \mathbf{h}_B)}{\partial \mathbf{h}_B^*} \left[\frac{\partial \ln p(\mathbf{y}, \mathbf{h}_B)}{\partial \mathbf{h}_B^*} \right]^H \right\} \in \mathbb{C}^{L_B \times L_B}. \quad (49)$$

The Bayesian CRLB is given by $\text{BCRLB}(\mathbf{h}_B) = \text{trace}(\mathcal{B}^{-1})$.

By resorting to the conditional expectation rule [42], the BIM (49) can be equivalently written as

$$\mathcal{B} = \mathbb{E}_{\mathbf{h}_B} \left\{ \mathbb{E}_{\mathbf{y}|\mathbf{h}_B} \left\{ \frac{\partial \ln p(\mathbf{y}, \mathbf{h}_B)}{\partial \mathbf{h}_B^*} \left[\frac{\partial \ln p(\mathbf{y}, \mathbf{h}_B)}{\partial \mathbf{h}_B^*} \right]^H \mid \mathbf{h}_B \right\} \right\} \quad (50)$$

Since $p(\mathbf{y}, \mathbf{h}_B) = p(\mathbf{y} | \mathbf{h}_B) p(\mathbf{h}_B)$, the second expectation in (50) becomes

$$\begin{aligned} \mathbb{E}_{\mathbf{y}|\mathbf{h}_B} \left\{ \frac{\partial \ln p(\mathbf{y}, \mathbf{h}_B)}{\partial \mathbf{h}_B^*} \left[\frac{\partial \ln p(\mathbf{y}, \mathbf{h}_B)}{\partial \mathbf{h}_B^*} \right]^H \mid \mathbf{h}_B \right\} \\ = \mathcal{B}_c + \frac{\partial \ln p(\mathbf{h}_B)}{\partial \mathbf{h}_B^*} \left[\frac{\partial \ln p(\mathbf{h}_B)}{\partial \mathbf{h}_B^*} \right]^H \end{aligned} \quad (51)$$

with

$$\mathcal{B}_c \triangleq \mathbb{E}_{\mathbf{y}|\mathbf{h}_B} \left\{ \frac{\partial \ln p(\mathbf{y} | \mathbf{h}_B)}{\partial \mathbf{h}_B^*} \left[\frac{\partial \ln p(\mathbf{y} | \mathbf{h}_B)}{\partial \mathbf{h}_B^*} \right]^H \mid \mathbf{h}_B \right\}. \quad (52)$$

Remembering that $\mathbf{h}_B \sim \mathcal{CN}(\mathbf{0}_{L_B}, \mathbf{I}_{L_B})$ by assumption, it results that $\partial \ln p(\mathbf{h}_B) / \partial \mathbf{h}_B^* = \mathbf{h}_B$, thus yielding

$$\mathcal{B} = \mathbb{E}_{\mathbf{h}_B} [\mathcal{B}_c] + \mathbf{I}_{L_B}. \quad (53)$$

On the other hand, since $\mathbf{d} \sim \mathcal{CN}(\mathbf{0}_N, \mathbf{R}_{dd})$, one gets

$$\frac{\partial \ln p(\mathbf{y} | \mathbf{h}_B)}{\partial \mathbf{h}_B^*} = -\mathbf{K}_B^H \mathbf{R}_{dd}^{-1} \mathbf{y} + \mathbf{K}_B^H \mathbf{R}_{dd}^{-1} \mathbf{K}_B \mathbf{h}_B. \quad (54)$$

Accounting for (54), the matrix \mathcal{B}_c defined in (52) can be expressed as $\mathcal{B}_c = \mathbf{K}_B^H \mathbf{R}_{dd}^{-1} \mathbf{K}_B$, which does not depend on \mathbf{h}_B . Therefore, owing to (53), it results that $\text{BCRLB}(\mathbf{h}_B)$ exactly coincides with (24).

APPENDIX D

PROOF OF LEMMA 4.1

By virtue of the matrix inversion lemma [22], one has

$$\begin{aligned} (\mathbf{I}_{L_B} + \mathbf{K}_B^H \mathbf{R}_{dd}^{-1} \mathbf{K}_B)^{-1} &= \mathbf{I}_{L_B} - \mathbf{K}_B^H (\mathbf{K}_B \mathbf{K}_B^H + \mathbf{R}_{dd}) \mathbf{K}_B \\ &= \mathbf{I}_{L_B} - \mathbf{J}^T \mathbf{K} (\mathbf{K} \mathbf{K}^H + \sigma_v^2 \mathbf{I}_N) \mathbf{K} \mathbf{J} \end{aligned} \quad (55)$$

where we have also used the expression of \mathbf{R}_{dd} and defined $\mathbf{J} \triangleq [\mathbf{I}_{L_B}, \mathbf{O}_{L_B \times L_E}]^T$ and $\mathbf{K} \triangleq [\mathbf{K}_B, \mathbf{K}_E] \in \mathbb{C}^{N \times (L_B + L_E)}$. By substituting (55) in (24) and using the limit formula for the Moore–Penrose inverse [20], one has

$$\overline{\text{BMSE}}_{\text{MMSE}} = L_B - \text{trace} \left[\mathbf{J}^T (\mathbf{K}^\dagger \mathbf{K})^H \mathbf{J} \right] \quad (56)$$

from which follows that $\overline{\text{BMSE}}_{\text{MMSE}} = 0$ if \mathbf{K} has full-column rank, i.e., $\mathbf{K}^\dagger \mathbf{K} = \mathbf{I}_{L_B}$. The proof is completed by observing that \mathbf{K} is full column rank if and only if the columns of \mathbf{A}_B and \mathbf{A}_E are linearly independent.

APPENDIX E TRUNCATED DISTRIBUTIONS

A real-valued random variable X is said to follow a *truncated Gaussian distribution* over the interval $[a, b]$ (with $b > a$) – denoted as $X \sim \mathcal{N}_T(\mu, \sigma, a, b)$ – if its pdf is given by (see, e.g., [46])

$$p_X(x) = \begin{cases} \frac{1}{C\sqrt{2\pi}\sigma} e^{-\frac{(x-\mu)^2}{2\sigma^2}}, & \text{for } a \leq x \leq b, \\ 0, & \text{otherwise,} \end{cases} \quad (57)$$

where μ and σ are the mean and standard deviation of the corresponding untruncated Gaussian distribution, respectively, and $C \triangleq \{\text{erf}[(b-\mu)/(\sqrt{2}\sigma)] - \text{erf}[(a-\mu)/(\sqrt{2}\sigma)]\}/2$ ensures that $p_X(x)$ is a valid pdf. It is important to emphasize that μ and σ are shape parameters for the truncated distribution – they are not the mean and the standard deviation of X . In the special case of $a = -b < 0$ and $\mu = 0$, it follows [46] that $\mathbb{E}[X] = 0$ and $\mathbb{E}[X^2] = \sigma^2 [1 - 2bp_X(b)]$.

Let $X \sim \mathcal{N}_T(\mu, \sigma, a, b)$, the random variable $Y = e^X$ exhibits a *truncated lognormal distribution*, i.e., its pdf can be written as

$$p_Y(y) = \begin{cases} \frac{1}{C\sqrt{2\pi}\sigma y} e^{-\frac{[\ln(y)-\mu]^2}{2\sigma^2}}, & \text{for } e^a \leq y \leq e^b, \\ 0, & \text{otherwise.} \end{cases} \quad (58)$$

In the special case of $a = -b < 0$ and $\mu = 0$, one has (details are omitted for the sake of brevity)

$$\begin{aligned} \mathbb{E}[Y] &= \mathbb{E}[e^X] = \mathbb{E}[e^{-X}] \\ &= \frac{e^{\frac{\sigma^2}{2}}}{2 \text{erf}\left(\frac{b}{\sqrt{2}\sigma}\right)} \left[\text{erf}\left(\frac{b-\sigma^2}{\sqrt{2}\sigma}\right) + \text{erf}\left(\frac{b+\sigma^2}{\sqrt{2}\sigma}\right) \right]. \end{aligned} \quad (59)$$

It is noteworthy that $\mathbb{E}[Y] = 1$, as $\sigma \rightarrow 0$.

APPENDIX F CASE 2: DERIVATION OF THE IMPROVED LMMSEE

The general expression of the LMMSEE [19] is given by

$$\hat{\mathbf{h}}_{\text{B,LMMSE}}^{(2)} = \mathbb{E}[\mathbf{h}_B \mathbf{y}^H] (\mathbb{E}[\mathbf{y} \mathbf{y}^H])^{-1} \mathbf{y} \quad (60)$$

where the expectation is taken not only over $(\mathbf{h}_B, \mathbf{h}_E, \mathbf{v})$, but over the probability densities of $\Delta\theta_{E,1}, \Delta\theta_{E,2}, \dots, \Delta\theta_{E,L_E}$, and $\Delta\mathcal{P}_E$ as well. It is readily seen that $\mathbb{E}[\mathbf{h}_B \mathbf{y}^H] = \mathbf{K}_B^H$.

By resorting to the conditional expectation rule [42], the correlation matrix in (60) can be equivalently written as

$$\begin{aligned} \mathbb{E}[\mathbf{y} \mathbf{y}^H] &= \mathbb{E}_{\{\Delta\theta_{E,\ell}\}_{\ell=1}^{L_E}, \Delta\mathcal{P}_E}[\mathbf{R}_{\mathbf{y}\mathbf{y}}] \\ &= \mathbf{K}_B \mathbf{K}_B^H + \mathbb{E}_{\{\Delta\theta_{E,\ell}\}_{\ell=1}^{L_E}, \Delta\mathcal{P}_E}[\mathbf{K}_E \mathbf{K}_E^H] + \sigma_v^2 \mathbf{I}_N \end{aligned} \quad (61)$$

where the (conditional) correlation matrix $\mathbf{R}_{\mathbf{y}\mathbf{y}}$, given \mathbf{K}_E , has been defined in (18). According to (30) and (31), we remember that $\mathbf{K}_E = \sqrt{\mathcal{P}_E} \mathbf{A}_E$, with $\mathcal{P}_E = \hat{\mathcal{P}}_E e^{-\Delta\mathcal{P}_E}$ and

$$\mathbf{A}_E = \frac{1}{\sqrt{L_E}} \begin{bmatrix} \mathbf{a}(\hat{\theta}_{E,1} - \Delta\theta_{E,1}), \mathbf{a}(\hat{\theta}_{E,2} - \Delta\theta_{E,2}), \\ \dots, \mathbf{a}(\hat{\theta}_{E,L_E} - \Delta\theta_{E,L_E}) \end{bmatrix}. \quad (62)$$

Using the properties of the Kronecker product, one gets

$$\begin{aligned} \mathbb{E}_{\{\Delta\theta_{E,\ell}\}_{\ell=1}^{L_E}, \Delta\mathcal{P}_E}[\mathbf{K}_E \mathbf{K}_E^H] \\ = \hat{\mathcal{P}}_E \mathbb{E}[e^{-\Delta\mathcal{P}_E}] \mathbb{E}_{\{\Delta\theta_{E,\ell}\}_{\ell=1}^{L_E}}[\mathbf{A}_E \mathbf{A}_E^H] \\ = \hat{\mathcal{P}}_E \mathbb{E}[e^{-\Delta\mathcal{P}_E}] \frac{1}{L_E} \sum_{\ell=1}^{L_E} \mathbf{R}_{\mathbf{a}\mathbf{a}}^{(\ell)} \end{aligned} \quad (63)$$

where we have defined

$$\mathbf{R}_{\mathbf{a}\mathbf{a}}^{(\ell)} \triangleq \mathbb{E}_{\Delta\theta_{E,\ell}}[\mathbf{a}(\hat{\theta}_{E,\ell} - \Delta\theta_{E,\ell}) \mathbf{a}^H(\hat{\theta}_{E,\ell} - \Delta\theta_{E,\ell})]. \quad (64)$$

By virtue of (59), it is readily seen that $\mathbb{E}[e^{-\Delta\mathcal{P}_E}]$ is given by (39). The $(n_1 + 1, n_2 + 1)$ th entry of $\mathbf{R}_{\mathbf{a}\mathbf{a}}^{(\ell)}$ is given by

$$\begin{aligned} \left\{ \mathbf{R}_{\mathbf{a}\mathbf{a}}^{(\ell)} \right\}_{n_1+1, n_2+1} &= \frac{\mathbb{E}_{\Delta\theta_{E,\ell}}[e^{-j2\pi(n_1-n_2)\Delta \cos(\hat{\theta}_{E,\ell} - \Delta\theta_{E,\ell})}]}{N} \\ &= \frac{\mathbb{E}_{\Delta\theta_{E,\ell}}\left\{ \cos\left[2\pi(n_1-n_2)\Delta \cos(\hat{\theta}_{E,\ell} - \Delta\theta_{E,\ell})\right] \right\}}{N} \\ &\quad - j \frac{\mathbb{E}_{\Delta\theta_{E,\ell}}\left\{ \sin\left[2\pi(n_1-n_2)\Delta \cos(\hat{\theta}_{E,\ell} - \Delta\theta_{E,\ell})\right] \right\}}{N} \end{aligned} \quad (65)$$

for $n_1, n_2 \in \{0, 1, \dots, N-1\}$. By resorting to the difference formula for cosine, one gets

$$\begin{aligned} \cos(\hat{\theta}_{E,\ell} - \Delta\theta_{E,\ell}) &= \cos(\hat{\theta}_{E,\ell}) \cos(\Delta\theta_{E,\ell}) \\ &\quad + \sin(\hat{\theta}_{E,\ell}) \sin(\Delta\theta_{E,\ell}) \\ &\approx \cos(\hat{\theta}_{E,\ell}) \left[1 - \frac{(\Delta\theta_{E,\ell})^2}{2} \right] + \sin(\hat{\theta}_{E,\ell}) \Delta\theta_{E,\ell} \end{aligned} \quad (66)$$

where we have also approximated $\cos(\Delta\theta_{E,\ell})$ and $\sin(\Delta\theta_{E,\ell})$ by using their corresponding second-order Maclaurin series expansion, under the assumption that the estimation error is sufficiently small. By substituting (66) in (65), employing the difference formulas for cosine and sine, taking second-order Maclaurin series expansion of $\cos[\beta_I(n_1, n_2, \ell) (\Delta\theta_{E,\ell})^2/2]$, $\cos[\beta_Q(n_1, n_2, \ell) \Delta\theta_{E,\ell}]$, $\sin[\beta_I(n_1, n_2, \ell) (\Delta\theta_{E,\ell})^2/2]$, $\sin[\beta_Q(n_1, n_2, \ell) \Delta\theta_{E,\ell}]$, and neglecting all the terms that tend to zero faster than $(\Delta\theta_{E,\ell})^2$, one has the approximations

$$\begin{aligned} \cos\left[2\pi(n_1-n_2)\Delta \cos(\hat{\theta}_{E,\ell} - \Delta\theta_{E,\ell})\right] &\approx \cos[\beta_I(n_1, n_2, \ell)] \\ &\quad \cdot \left[1 - \beta_Q^2(n_1, n_2, \ell) \frac{(\Delta\theta_{E,\ell})^2}{2} \right] + \sin[\beta_I(n_1, n_2, \ell)] \\ &\quad \cdot \left[\beta_I(n_1, n_2, \ell) \frac{(\Delta\theta_{E,\ell})^2}{2} - \beta_Q(n_1, n_2, \ell) \Delta\theta_{E,\ell} \right] \end{aligned} \quad (67)$$

$$\begin{aligned} \sin \left[2\pi(n_1 - n_2)\Delta \cos(\hat{\theta}_{E,\ell} - \Delta\theta_{E,\ell}) \right] &\approx \sin [\beta_I(n_1, n_2, \ell)] \\ &\cdot \left[1 - \beta_Q^2(n_1, n_2, \ell) \frac{(\Delta\theta_{E,\ell})^2}{2} \right] - \cos [\beta_I(n_1, n_2, \ell)] \\ &\cdot \left[\beta_I(n_1, n_2, \ell) \frac{(\Delta\theta_{E,\ell})^2}{2} - \beta_Q(n_1, n_2, \ell) \Delta\theta_{E,\ell} \right] \quad (68) \end{aligned}$$

where $\beta_I(n_1, n_2, \ell) \triangleq 2\pi(n_1 - n_2)\Delta \cos(\hat{\theta}_{E,\ell})$ and $\beta_Q(n_1, n_2, \ell) \triangleq 2\pi(n_1 - n_2)\Delta \sin(\hat{\theta}_{E,\ell})$. Eq. (38) comes from taking the expectation of (67) and (68) over the pdf of $\Delta\theta_{E,\ell}$ (see Appendix E) and substituting the results in (65).

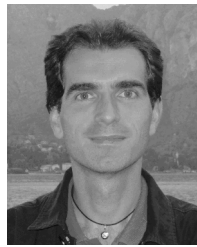
REFERENCES

- [1] I.E. Telatar, "Capacity of multi-antenna Gaussian channels," *Eur. Trans. Telecommun.*, vol. 10, pp. 585–595, Nov./Dec. 1999.
- [2] G.J. Foschini, "Layered space-time architecture for wireless communication in a fading environment when using multi-element antennas," *Bell Labs Tech. J.*, pp. 41–59, Autumn 1996.
- [3] G.J. Foschini and M.J. Gans, "On limits of wireless communications in a fading environment when using multiple antennas," *Wireless Personal Commun.*, vol. 6, pp. 311–335, 1998.
- [4] D. Darsena, G. Gelli, and F. Verde, "Precoding/Beamforming," *Wiley 5G Ref.*, Jan. 2020.
- [5] R. Miller and W. Trappe, "On the vulnerabilities of CSI in MIMO wireless communication systems," *IEEE Trans. Mobile Comput.*, vol. 11, pp. 1386–1398, Aug. 2012.
- [6] X. Zhou, B. Maham, and A. Hjørungnes, "Pilot contamination for active eavesdropper," *IEEE Trans. Wireless Commun.*, vol. 11, pp. 903–907, Feb. 2012.
- [7] D. Kapetanovic, G. Zheng, K.-K. Wong, and B. Ottersten, "Detection of pilot contamination attack using random training and massive MIMO," in *Proc. IEEE Int. Symp. on Personal, Indoor and Mobile Radio Commun.*, London, UK, Sep. 2013, pp. 13–18.
- [8] S. Im, H. Jeon, J. Choi, and J. Ha, "Secret key agreement with large antenna arrays under the pilot contamination attack," *IEEE Trans. Wireless Commun.*, vol. 14, pp. 6579–6594, Dec. 2015.
- [9] Q. Xiong, Y.-C. Liang, K.H. Li, and Y. Gong, "An energy-ratio-based approach for detecting pilot spoofing attack in multiple-antenna systems," *IEEE Trans. Inf. Foren. Sec.*, vol. 10, pp. 932–940, May 2015.
- [10] Y.O. Basciftci, C.E. Koksak, and A. Ashikhmin, "Securing massive MIMO at the physical layer," *IEEE Conference on Communications and Network Security (CNS)*, Florence, Italy, Sep. 2015, pp. 272–280.
- [11] J.K. Tugnait, "Self-contamination for detection of pilot contamination attack in multiple antenna systems," *IEEE Wireless Commun. Lett.*, vol. 4, pp. 525–528, Oct. 2015.
- [12] Q. Xiong, Y.-C. Liang, K.H. Li, Y. Gong, and S. Han, "Secure transmission against pilot spoofing attack: A two-way training-based scheme," *IEEE Trans. Inf. Foren. Sec.*, vol. 11, pp. 1017–1026, May 2016.
- [13] Y. Wu, R. Schober, D.W.K. Ng, C. Xiao, and G. Caire, "Secure massive MIMO transmission with an active eavesdropper," *IEEE Trans. Inf. Foren. Sec.*, vol. 62, pp. 3880–3900, Jul. 2016.
- [14] J.K. Tugnait, "Detection and identification of spoofed pilots in TDD/SDMA systems," *IEEE Wireless Commun. Lett.*, vol. 6, pp. 550–553, Aug. 2017.
- [15] J.K. Tugnait, "Pilot spoofing attack detection and countermeasure," *IEEE Trans. Commun.*, vol. 66, pp. 2093–2105, May 2018.
- [16] H.-M. Wang, K.-W. Huang, and T.A. Tsiftsis, "Multiple antennas secure transmission under pilot spoofing and jamming attack," *IEEE J. Select. Areas Commun.*, vol. 36, pp. 860–876, Apr. 2018.
- [17] K.-W. Huang, H.-M. Wang, Y. Wu, and R. Schober, "Pilot spoofing attack by multiple eavesdroppers," [Online]. Available: <http://arxiv.org/abs/1505.00396>.
- [18] W. Wang *et al.*, "On countermeasures of pilot spoofing attack in massive MIMO systems: A double channel training based approach," *IEEE Trans. Veh. Technol.*, vol. 68, pp. 6697–6708, July 2019.
- [19] S.M. Kay, *Fundamentals of Statistical Signal Processing: Estimation Theory*. Englewood Cliffs, NJ: Prentice-Hall, 1993.
- [20] A. Ben-Israel and T.N.E. Greville, *Generalized Inverses*. New York, NY, USA: Springer-Verlag, 2002.
- [21] J.G. Proakis, *Digital Communications*. New York: McGraw-Hill, 2001.
- [22] R.A. Horn and C.R. Johnson, *Topics in Matrix Analysis*. U.K.: Cambridge Univ. Press, 1991.
- [23] R.A. Horn and C.R. Johnson, *Matrix Analysis*. New York: Cambridge Univ. Press, 1990.
- [24] A. Hjørungnes and D. Gesbert, "Complex-valued matrix differentiation: techniques and key results," *IEEE Trans. Signal Process.*, vol. 55, pp. 2740–2746, June 2007.
- [25] M. Buehner and A.B. Gershman, "Training-based MIMO channel estimation: A study of estimator tradeoffs and optimal training signals," *IEEE Trans. Signal Process.*, vol. 54, pp. 884–893, Mar. 2006.
- [26] R.B. Ertel, P. Cardieri, K.W. Sowerby, T.S. Rappaport, and J.H. Reed, "Overview of spatial channel models for antenna array communication systems," *IEEE Personal Commun.*, vol. 5, pp. 10–22, Feb. 1998.
- [27] Y. Ding and V. Fusco, "Orthogonal vector approach for synthesis of multi-beam directional modulation transmitters," *IEEE Antennas Wireless Propag. Lett.*, vol. 14, pp. 1330–1333, Feb. 2015.
- [28] E. Tuncer and B. Friedlander, *Classical and Modern Direction-of-Arrival Estimation*. Academic Press, 2009.
- [29] Z. Chen, G. Gokeda, and Y. Yu, *Introduction to Direction-of-Arrival Estimation*. Artech House, 2010.
- [30] S. Chandran, *Advances in Direction-of-Arrival Estimation*. Artech House, 2006.
- [31] A. Innok, P. Uthansakul, and M. Uthansakul, "Angular beamforming technique for MIMO beamforming system," *Int. J. Antennas and Propag.*, volume 2012, article ID 638150, 10 pages.
- [32] G.H. Golub and C.F. Van Loan, *Matrix Computations*. Baltimore, MD: John Hopkins Univ. Press, 1996.
- [33] H.L. Van Trees, *Detection and Modulation Theory*. New York: Wiley, 1968, vol. 1.
- [34] M. Dong and L. Tong, "Optimal design and placement of pilot symbols for channel estimation," *IEEE Trans. Signal Process.*, vol. 50, pp. 3055–3069, Dec. 2002.
- [35] L. Du, J. Li, P. Stoica, "Fully automatic computation of diagonal loading levels for robust adaptive beamforming," *IEEE Trans. Aerosp. Electron. Syst.*, vol. 46, pp. 449–458, Jan. 2010.
- [36] M. Wax and T. Kailath, "Detection of signals by information theoretic criteria," *IEEE Trans. Acoustics Speech Signal Proc.*, vol. 33, pp. 387–392, April 1985.
- [37] H.L. Van Trees, *Optimum Array Processing (Detection, Estimation, and Modulation Theory, Part IV)*, John Wiley & Sons, New York, NY, USA, 2002.
- [38] P. Stoica and A. Nehorai, "MUSIC, maximum likelihood, and Cramér-Rao bound," *IEEE Trans. Acoustics Speech Signal Proc.*, vol. 37, pp. 720–741, May 1989.
- [39] R. Roy and T. Kailath, "ESPRIT-estimation of signal parameters via rotational invariance techniques," *IEEE Trans. Acoustics Speech Signal Proc.*, vol. 37, pp. 984–995, July 1989.
- [40] J.-A. Tsai, R.M. Buehrer, and B.D. Woerner, "BER performance of a uniform circular array versus a uniform linear array in a mobile radio environment," *IEEE Trans. Wireless Commun.*, vol. 3, pp. 695–700, May 2004.
- [41] A.J. Goldsmith, L. Greenstein, and G. Foschini, "Error statistics of real-time power measurements in cellular channels with multipath and shadowing," *IEEE Trans. Veh. Technol.*, vol. 43, pp. 439–446, Aug. 1994.
- [42] G. Casella and R.L. Berger, *Statistical Inference*. Pacific Grove, CA: Duxbury/Thompson Learning, 2002.
- [43] S.K. Leung-Yan-Cheong and M.E. Hellman, "The Gaussian wire-tap channel," *IEEE Trans. Inf. Theory*, vol. 24, pp. 451–456, July 1978.
- [44] M. Joham, W. Utschick, and J. Nosske, "Linear transmit processing in MIMO communications systems," *IEEE Trans. Signal Process.*, vol. 53, pp. 2700–2712, Aug. 2005.
- [45] A.W. Marshall, I. Olkin, and B.C. Arnold, *Inequalities: Theory of Majorization and Its Applications (2nd ed.)*. New York: Springer, 2011.
- [46] N. Johnson, S. Kotz, and N. Balakrishnan, *Continuous Univariate Distributions*, Second Edition, Wiley, 1994.



Donatella Darsena (M'06-SM'16) received the Dr. Eng. degree *summa cum laude* in telecommunications engineering in 2001, and the Ph.D. degree in electronic and telecommunications engineering in 2005, both from the University of Napoli Federico II, Italy. From 2001 to 2002, she was an engineer in the Telecommunications, Peripherals and Automotive Group, STMicroelectronics, Milano, Italy. Since 2005, she has been an Assistant Professor with the Department of Engineering, University of Napoli Parthenope, Italy. Her research activities lie

in the area of statistical signal processing, digital communications, and communication systems. In particular, her current interests are focused on equalization, channel identification, narrowband-interference suppression for multicarrier systems, space-time processing for cooperative communications systems and cognitive communications systems, and software-defined networks. Dr. Darsena has served as an Associate Editor for the IEEE COMMUNICATIONS LETTERS since December 2016, Senior Area Editor of the IEEE COMMUNICATIONS LETTERS since 2019 and Associate Editor for IEEE Access since October 2018



Francesco Verde (M'10-SM'14) was born in Santa Maria Capua Vetere, Italy, on June 12, 1974. He received the Dr. Eng. degree *summa cum laude* in electronic engineering from the Second University of Napoli, Italy, in 1998, and the Ph.D. degree in information engineering from the University of Napoli Federico II, in 2002. Since December 2002, he has been with the University of Napoli Federico II. He first served as an Assistant Professor of signal theory and mobile communications and, since December 2011, he has served as an Associate Pro-

fessor of telecommunications with the Department of Electrical Engineering and Information Technology. His research activities include orthogonal/non-orthogonal multiple-access techniques, space-time processing for cooperative/cognitive communications, wireless systems optimization, and software-defined networks.

Prof. Verde has been involved in several technical program committees of major IEEE conferences in signal processing and wireless communications. He has served as Associate Editor for IEEE TRANSACTIONS ON COMMUNICATIONS since 2017 and Senior Area Editor of the IEEE SIGNAL PROCESSING LETTERS since 2018. He was an Associate Editor of the IEEE TRANSACTIONS ON SIGNAL PROCESSING (from 2010 to 2014) and IEEE SIGNAL PROCESSING LETTERS (from 2014 to 2018), as well as Guest Editor of the EURASIP Journal on Advances in Signal Processing in 2010 and SENSORS MDPI in 2018.



Giacinto Gelli (M'18, SM'20) was born in Napoli, Italy, on July 29, 1964. He received the Dr. Eng. degree *summa cum laude* in electronic engineering in 1990, and the Ph.D. degree in computer science and electronic engineering in 1994, both from the University of Napoli Federico II.

From 1994 to 1998, he was an Assistant Professor with the Department of Information Engineering, Second University of Napoli. Since 1998 he has been with the Department of Electrical Engineering and Information Technology, University of Napoli

Federico II, first as an Associate Professor, and since November 2006 as a Full Professor of Telecommunications. He also held teaching positions at the University Parthenope of Napoli. His research interests are in the broad area of signal and array processing for communications, with current emphasis on backscatter communications, multicarrier modulation systems and space-time techniques for cooperative and cognitive communications systems.



Ivan Iudice was born in Livorno, Italy, on November 23, 1986. He received the B.S. and M.S. degrees in telecommunications engineering in 2008 and 2010, respectively, and the Ph.D. degree in information technology and electrical engineering in 2017, all from University of Napoli Federico II, Italy.

Since 2011, he has been part of the Electronics and Communications laboratory at Italian Aerospace Research Centre (CIRA), Capua, Italy. His research activities lie in the area of signal and array process-

ing for communications, with current interests are focused on physical layer cyber security and space-time techniques for cooperative communications systems.